August 1, 2016

# Technical Memorandum

To: Chris Misenis, WACOR, EPA/OAR/OAQPS/AQAD
Zac Adelman, UNC/Institute for the Environment

From: Chris Emery, Bonyoung Koo, Wei Chun Hsieh, Andy Wentland, Gary Wilson, Greg Yarwood

Project: EPA Contract EPD12044; WA 4-07: Meteorological, Photochemical, and Dispersion Modeling Support
**Task 7: Update Carbon Bond Chemical Mechanism**

---

## Summary

Ramboll Environ (RE) revised version 6 of the Carbon Bond mechanism (CB6) by combining two existing updates to CB6 revision 2 (CB6r2). CB6r3 implemented temperature and pressure dependent yields of organic nitrates for alkanes larger than ethane (Emery et al., 2015). A compact reaction mechanism called "I-16b" represents ozone depletion by iodine in the marine boundary layer (Emery et al., 2016). The new mechanism called CB6r4 combines CB6r3 with I-16b and has been implemented in the Comprehensive Air Quality Model with extension (CAMx) version 6.32. We include a brief summary of model tests and comparisons of model performance against CB6r2, considered the CAMx standard to date. We also include documentation on our standard benchmark testing and quality assurance protocol conducted for each public distribution of the CAMx code. The report concludes with user instructions on configuring CAMx to run the updated mechanism. This interim version of CAMx (v6.32) is being delivered to EPA with this report as a deliverable for Task 7 of Work Assignment 4-07. RE will coordinate with EPA's CMAQ developers to install CB6r4 into CMAQ.

## Background

RE publicly released CAMx v6.30 in April 2016 (Ramboll Environ, 2016) with several Carbon Bond mechanisms: CB05 is retained for backwards compatibility but should be phased-out; CB6r2 is the standard version and was first released in CAMx v6.10, April 2014; CB6r2h adds halogen reactions for iodine, bromine and chlorine compounds and was first released in CAMx v6.20, March 2015); and CB6r3 with pressure and temperature dependent organic nitrate yields from alkanes is new in CAMx v6.30.

CB6r3 was developed to better represent alkyl nitrate formation from alkanes in cold conditions and at lower atmospheric pressures that are relevant to wintertime, high altitude conditions of western oil and gas basins (Emery et al., 2015). Alkyl nitrate yields in CB6r3 are

the same as CB6r2 at 298 K and 1 atm so that the mechanisms perform similarly for summer ozone conditions.

Halogen reactions were included in CB6r2h to investigate ozone depletion in marine environments such as Gulf of Mexico (Yarwood et al., 2014). The extra computational burden of CB6r2h motivated subsequent development of a compact iodine mechanism that includes the 16 most important reactions of inorganic iodine and is called I-16b (Emery et al., 2016). Implementation of I-16b in CAMx v6.31 is supported by a new in-line iodine emissions parameterization that computes inorganic iodine emissions caused by ozone deposition to seawater (Garland and Curtis, 1981).

In this Work Assignment RE combined CB6r3 and the I-16b compact iodine mechanism into a single revised Carbon Bond mechanism called CB6r4, and implemented it in CAMx v6.32. The CAMx Ozone and PM Source Apportionment Technology (OSAT and PSAT, or collectively SA) modules have been updated to account for ozone destruction by halogens and changes to nitrogen tracer classes that account for halogen species that also contain nitrogen.

## Developing CB6r4

### CB6r3 Description

Alkyl nitrates ($RONO_2$) can influence ozone production because both nitric oxide (NO) and radicals (specifically $RO_2$) are removed by alkyl nitrate formation. However, the temperature dependence of alkyl nitrate formation is omitted from current photochemical mechanisms such as CB05-TU (Whitten et al., 2010), CB6r2 (Hildebrandt Ruiz and Yarwood, 2013), SAPRC11 (Carter and Heo, 2013), RACM2 (Goliff et al., 2013) and the Master Chemical Mechanism (Saunders et al., 2003). Lee et al. (2014) considered how cold winter conditions affect alkyl nitrate branching and concluded that omitting the temperature dependence may cause a 15% high bias in ozone formation.

Alkyl nitrates are formed when alkanes are oxidized in the atmosphere in the presence NO. Alkanes are compounds of hydrogen and carbon with only single bonds connecting the atoms, e.g., methane ($CH_4$), ethane ($C_2H_6$), propane ($C_4H_8$), etc. Analyses of air samples collected in western US oil and gas development basins during wintertime ozone events show that alkanes dominate the organic gases present in the air. The formation of alkyl nitrates from alkanes can be described by the following reactions in which an alkane (RH) reacts with hydroxyl radical (HO) and oxygen ($O_2$) to form an alkyl peroxy radical ($RO_2$) that has two potential reaction pathways with $NO^{\bullet}$:

| | | |
|---|---|---|
| 1) | $HO + RH$ | $\rightarrow R + H_2O$ |
| 2) | $R + O_2$ | $\rightarrow RO_2$ |
| 3a) | $RO_2 + NO$ | $\rightarrow RONO_2$ |
| 3b) | | $\rightarrow RO + NO_2$ |

Perring et al. (2013) have reviewed the atmospheric impacts of $RONO_2$ formation. The yield of $RONO_2$ is determined by the branching ratio between reactions 3a and 3b, which depends on both temperature and pressure (Atkinson et al., 1983). The association reaction of $RO_2$ with NO in reaction 3a is favored over reaction 3b by lower temperatures and higher pressures.

RE developed the CB6r3 chemical mechanism from CB6r2 to improve applicability to winter conditions (Emery et al., 2015). Temperature and pressure dependent formation of $RONO_2$ was implemented for propane (CB6 species "PRPA") and larger alkanes (CB6 species "PAR") using the parameterization of Yeh and Ziemann (2014). CB6r3 was designed to produce the same $RONO_2$ yields as CB6r2 at room temperature and pressure (298 K and 1 atm). CAMx simulations with CB6r3 for the Uintah Basin of Utah confirmed the directionality of the ozone effect described by Lee et al. (2014)..

**Compact Iodine Mechanism (I-16b) Description**

CAMx and many other regional and global models have tended to over predict ozone in the Gulf of Mexico region (Yarwood et al., 2012). Iodine compounds emitted from ocean waters can cause ozone depletion of several ppb per day within the marine boundary layer (Mahajan et al., 2010 and references therein). Iodine depletes ozone catalytically, meaning that a single iodine atom can destroy many ozone molecules (Chameides and Davis, 1980; Mahajan et al., 2009). Emissions of inorganic iodine compounds ($I_2$ and HOI) are caused by deposition of ozone to ocean waters (Garland and Curtis, 1981; Carpenter et al., 2013), whereas emissions of organic iodine compounds result from biological processes (Carpenter, 2003).

Yarwood et al. (2014) incorporated halogen chemistry for iodine, bromine and chlorine to the CB6r2 chemical mechanism (CB6r2h), adding 88 more reactions to the original 216 (41% increase) and 33 more transported species to the original 75 (44% increase). In the Gulf of Mexico, ozone reductions using CB6r2h exceeded 6 ppb near the Texas coastline, mostly attributable to inorganic iodine. However, CAMx run times about doubled over CB6r2. RE recently developed a more efficient condensed halogen mechanism treating only inorganic iodine (Emery et al., 2016) and implemented a new in-line emissions algorithm that incorporates recent findings on the feedback between ozone deposition to ocean waters and emission flux of iodine (Prados-Roman et al., 2015; Garland and Curtis, 1981).

Following Prados-Roman et al. (2015), the CAMx in-line emissions algorithm incorporates the CAM-Chem parameterizations for aqueous iodine [$I^-_{aq}$] in ocean surface water, and $I_2$ and HOI (collectively referred to as "Ix") air emissions as a function of ozone air concentration, wind speed and sea surface temperature (SST). These emission fluxes are added as new fields to the CAMx deposition output files so that they can be plotted and analyzed. Aqueous iodide concentrations exhibit a strong exponential sensitivity to SST, resulting in similarly strong Ix emissions sensitivity to SST and wind speed and a linear Ix emissions response to ambient ozone concentrations. For conditions typical of the Gulf of Mexico, HOI contributes 91-99% of the total Ix emissions flux with $I_2$ contributing the remainder.

The iodine portion of CB6r2h includes 30 reactions (Yarwood et al., 2014). RE investigated the roles of these reactions through a comprehensive sensitivity analysis employing the Decoupled Direct Method (DDM). We identified a sub-group of key iodine reactions that are most important to the dynamics of the full iodine mechanism, and that are consistently the key drivers of ozone depletion across a range of Ix emission. We considered a subset of reactions that (1) have an aggregated sensitivity (ideally) equaling the full 30-reaction iodine mechanism, and (2) include all the essential reactions needed by the three catalytic iodine cycles involved as well as the dominating iodine sinks. A set of 16 reactions involving 9 inorganic iodine species were selected to form a compact mechanism referred to as "I-16b". The aggregated sensitivity with these reactions was 101% of the group sensitivity for the 30-reaction mechanism. Five reactions involving iodine-containing halomethanes were all eliminated. Several other reactions were also eliminated, considering their negligible impact on ozone and other species.

Emery et al. (2016) showed that the efficiency of ozone depletion by iodine is highly dependent on the amount of iodine enrichment; therefore, accurately representing important iodine precursors (e.g., HOI) is critical for the fidelity of simulating ozone depletion by iodine. In CAMx simulations for Texas, the full halogen and I-16b mechanisms produced similar peak ozone decrements of 5-7 ppb over the Gulf of Mexico. CAMx run times were reduced by 31% using I-16b relative to CB6r2h, but remained 56% longer than the CB6r2 mechanism without halogen chemistry. While I-16b is faster than CB6r2h, it remains disproportionately slow relative to CB6r2 because of stiff reactions involving I, IO and OIO species.

**The CB6r4 Mechanism**

The CB6r3 and I-16b mechanisms described above were combined into a single chemistry mechanism; the first developmental version of this mechanism is referred to as "CB6r4d1" and this name appears in some development testing results, below. CB6r4d1 also adds pseudo-heterogeneous hydrolysis of isoprene-derived organic nitrate (INTR). Aerosol uptake of organic nitrate followed by particle-phase hydrolysis to $HNO_3$ formation can be an important pathway for loss of atmospheric NOx (Hildebrandt Ruiz and Yarwood, 2013; Jacobs et al., 2014; Fisher et al., 2016). CB6r4 assumes the same lifetime (1 hour) against particle-phase hydrolysis of INTR as Fisher et al. (2016). Partitioning of organic nitrate into particle phase is modeled using a two-product parameterization based on ambient measurement data during the 2010 CalNex (Rollins et al., 2013). If PM is not explicitly modeled, equal partitioning between the gas and particle phases is assumed.

The final CB6r4 mechanism has two changes from CB6r4d1 (and from CB6r2). First, an error in the reaction of ISO2 with RO2 was corrected by changing the product yield of RO2 from 0.072 to 1.072. The corrected reaction reads:

ISO2 + RO2 = 0.598 FORM + 1.000 ISPD + 0.728 HO2 + 0.072 XO2H + 1.072 RO2

Second, all reactions of volatile organic compounds (VOC) with oxygen atoms (O) were deleted, namely:

- FORM + O = OH + HO2 + CO
- ALD2 + O = C2O3 + OH
- ALDX + O = CXO3 + OH
- ETH + O = FORM + HO2 + CO + 0.7 XO2H + 0.7 RO2 + 0.3 OH
- OLE + O = 0.2 ALD2 + 0.3 ALDX + 0.1 HO2 + 0.2 XO2H + 0.2 CO + 0.2 FORM + 0.01 XO2N + 0.21 RO2 + 0.2 PAR + 0.1 OH
- IOLE + O = 1.24 ALD2 + 0.66 ALDX + 0.1 XO2H + 0.1 RO2 + 0.1 CO + 0.1 PAR
- ISOP + O = 0.75 ISPD + 0.5 FORM + 0.25 XO2 + 0.25 RO2 + 0.25 HO2 + 0.25 CXO3 + 0.25 PAR
- TERP + O = 0.15 ALDX + 5.12 PAR

O-atom reactions of VOC were included in Carbon Bond mechanisms because they can matter for smog chamber simulations used for mechanism development, but they have negligible impact in atmospheric simulations. The final CB6r4 mechanism includes 229 reactions of 86 species. The full listing of CB6r4 is given in Appendix A.

The CAMx SA Probing Tool was coupled to CB6r4 and updated to account for an additional ozone destruction pathway by iodine and conversion of nitrogen tracer classes involving iodine nitrate (INO3).

**Chemistry Solver Speedups**

Previous testing of the I-16b mechanism (Emery et al., 2016) showed that the main Euler Backward Iterative (EBI) solver in CAMx converged slowly due to strong interactions between certain iodine species (i.e., stiffness). The CAMx EBI solver includes special subroutines to solve other groups of stiff species (e.g., HOx and NOx) using analytical solutions proposed by Hertel et al. (1993). We implemented and tested a Hertel-style solution for I and IO and results were accurate but not faster. We implemented an iterative EBI solution for the species I, IO and OIO together which was faster. We updated the chemical mechanism compiler (CMC) for CAMx to automatically apply this solver strategy (called the IOx solver) for CB6r4, CB6r2h and any future halogen mechanisms in CAMx. While developing the IOx solver we also restructured the loop over species in the main CAMx EBI solver to improve efficiency for all chemical mechanisms.

**Developmental Testing with a Texas Dataset**

We tested the impact of EBI solver speedup modifications and the elimination of VOC + O reactions on CAMx concentrations and speed in 3-D simulations. We used the same 3-day (June 16-18, 2006) period as Yarwood et al. (2014) and Emery et al. (2016) used to develop the CB6r2h and I-16b halogen mechanisms for the Texas Commission on Environmental Quality (TCEQ). Emissions of $I_2$ and HOI were generated by the in-line iodine emissions parameterization. Emission inputs of bromine, chlorine, and organic I compounds (needed by CB6r2h) and initial/boundary conditions were developed by Yarwood et al. (2014). All other model inputs were obtained from the TCEQ. All tests were run for the 36- and 12-km grids

covering the continental US and state of Texas, respectively, using 2-way grid nesting. These simulations did not include PM.

Three CAMx runs were conducted with CB6r4 variants:

- CB6r4d1 (orig) – CB6r4d1 with the original/unmodified EBI solver;
- CB6r4d1 (rev) – CB6r4d1 with the revised EBI solver (IOx solver and EBI restructuring);
- CB6r4 (rev) – CB6r4 with the revised EBI solver.

Figure 1 shows the maximum absolute differences in hourly surface ozone concentrations between CB6r4d1 (rev) and CB6r4d1 (orig), and between CB6r4 (rev) and CB6r4d1 (rev) for each simulation day. Ozone differences due to EBI solver revisions were less than 1 ppb over the whole modeling domain. Removing VOC + O reactions had much smaller impacts (< 0.1 ppb).

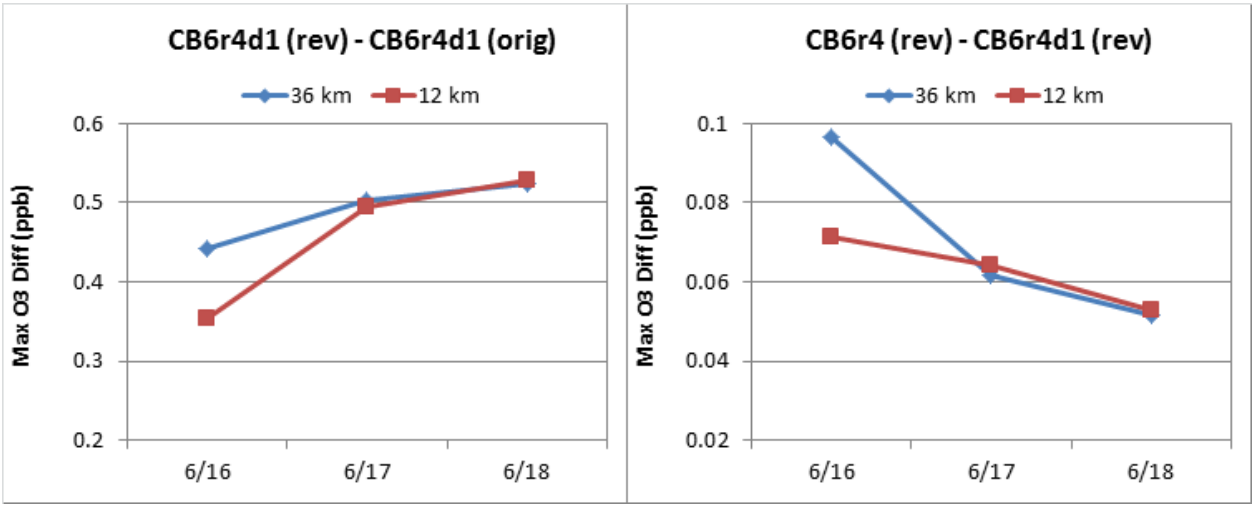


**Figure 1. Maximum absolute differences in hourly surface ozone concentrations (ppb) between CB6r4d1 (rev) and CB6r4d1 (orig) and between CB6r4 (rev) and CB6r4d1 (rev) on the 36- and 12-km grids.**

Figure 2 compares average runtimes per simulation day between the three test cases. The revised chemistry solver for I, IO and OIO reduced the average runtime by 17% for the CB6r4d1 mechanism. The revised chemistry solver was also implemented to solve Cl, ClO, Br, BrO, I, IO and OIO in CB6r2h and achieved a similar speed improvement (by 20%). Eliminating the 8 reactions of VOC with O in CB6r4 further reduced the runtime by an additional 3%.

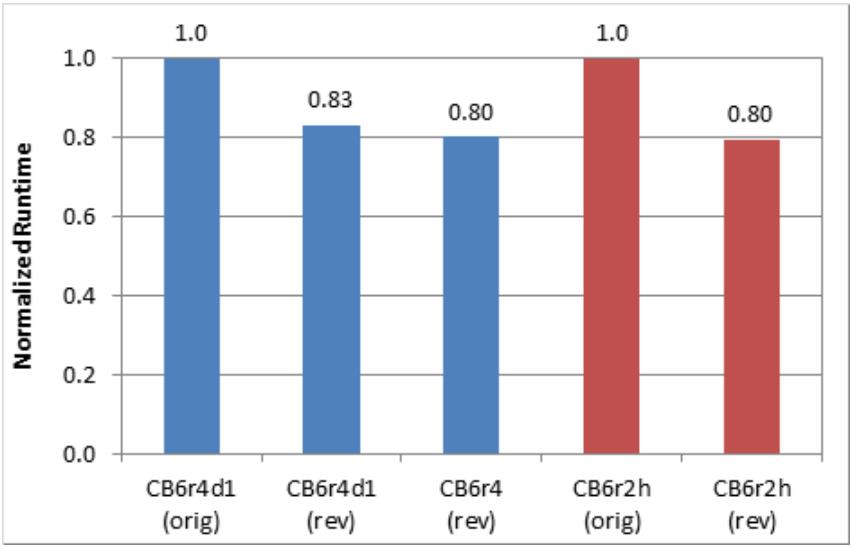


**Figure 2. Average 3-D simulation runtimes for CB6r4d1, CB6r4, and CB6r2h with the original (orig) and revised (rev) chemistry solvers; the runtime is normalized by that of the original solver.**

### Benchmarking Source Code for Distribution

Each individual update to the CAMx code is first tested by its author at a process level to ensure that the update is properly implemented and bug-free and that the model operates and responds correctly. The particular approach employed for testing depends to some degree on the affected process (emissions, chemistry, transport, removal, Plume-in-Grid, Probing Tools), the extent of code changes, and author preference. Tested modifications from all authors are then brought together into the CAMx code repository and committed into a new version using the "Git" revision control system. The updated model is then subjected to RE's standard internal benchmark testing and quality assurance protocol conducted for each public distribution of the code. The steps in this process are summarized below:

1. Compile CAMx using RE's installations of the latest versions of Portland Group Fortran (PGF90 v13.4), Intel Fortran (IFORT v15.0), and Gnu Fortran (GFORTRAN v4.4.7), with all parallelization options (OMP, MPI and OMP+MPI hybrid) to ensure no compile-time or library linking errors (9 separate executables).
2. Compile CAMx with array-bounds checking using PGF90 and IFORT and all parallelization options (6 separate executables). Run all 6 executables on RE's distributed test case (2-day period on 36 and 12 km grids centered over the central US) for the following matrix of cases:
   a) Multiple grid configurations (36 km only, 36+12 km);
   b) With and without Plume-in-Grid (PiG);
   c) All Carbon Bond chemical mechanisms available in the current CAMx version.
3. Run all 6 executables from Step 2 for all Probing Tools (SA, DDM, RTRAC, PA) and for all grid and PiG combinations.

4. Run all 9 executables from Step 1 on the distributed test case without PiG (unless PiG had been modified) using a standard chemistry mechanism. Compare all combinations of parallelization against a non-parallel (single-CPU) case with advection "super-stepping" turned off to verify equivalent results in all cases.
5. Repeat Step 4 for any Probing Tools that have been modified in the current version.
6. Graphically compare results from Steps 4 and 5 to previous benchmarking runs performed for the last CAMx version to verify consistency and understand differences; verify that major differences in concentration, deposition, and Probing Tool patterns can be explained on the basis of model updates and bug fixes.
7. Upon successful completion of all tests, update CAMx version and date statements in each code file (subroutines, include files, modules, utilities).

RE applied this protocol to CAMx v6.32 in preparation of delivery to EPA. Exceptions in this case included:

- Step 2 was conducted only for new CAMx Mechanism 4 (i.e., CB6r4) as all other mechanisms were previously tested as part of the distribution of v6.30;
- Steps 3 and 5 were conducted only for SA with CB6r4, as new processes were introduced for ozone decay and nitrogen tracers. DDM and PA will be tested subsequently with CB6r4; RTRAC was previously tested as part of the distribution of v6.30.

## Model Evaluation

RE ran CAMx on the EPA's 2011 Modeling Platform for a summer period (June-July) using CB6r2 and CB6r4, from which ozone differences and model performance statistics were evaluated on a regional basis. As expected, impacts to ozone were found to be minor (particularly at inland sites), with maximum hourly ozone impacts of 5-10 ppb along the Gulf Coast. Impacts to maximum daily 8-hour average (MDA8) ozone and PM were negligible from a statistical standpoint. Changes to hourly ozone model performance statistics (normalized mean bias and error) between CB6r2 and CB6r4 at rural and coastal monitoring sites throughout the CONUS domain are tabulated below.

### 2011 Modeling Platform

The 2011 Modeling Platform for CAMx (July 28, 2015 Notice of Data Availability or NODA) comprises a single expansive grid covering the continental US (CONUS) with 12 km grid spacing and extending vertically in 25 layers up to ~50 mb (~18-20 km). The dataset includes a full year of 2011 hourly meteorology and point/gridded anthropogenic and biogenic emissions (version "2011EH") speciated for the CB6 mechanism, initial and boundary conditions generated from the GEOS-Chem global chemical transport model, and other ancillary inputs.

We selected the test period to span June 20 – July 31, where the June period was used only for model spinup from a previous CAMx run. Model simulations employed CB6r2 (v6.30) and CB6r4 (v6.32) gas-phase chemistry, the 2-mode (CF) PM treatment, Zhang dry deposition and wet deposition; Plume-in-Grid and ACM2 boundary layer mixing were not invoked.

**AMET Configuration**

RE employed the Atmospheric Model Evaluation Tool (AMET) to calculate model performance statistics and generate various graphical evaluation products. Air concentration measurements were taken from three monitoring network datasets: the Air Quality System (AQS) network for hourly ozone; the Interagency Monitoring of Protected Visual Environments (IMPROVE) network for 24-hour speciated $PM_{2.5}$, and the Clean Air Status and Trends Network (CASTNet) for weekly speciated $PM_{2.5}$. Wet deposition was evaluated against weekly measurements from the National Acid Deposition and Program (NADP) network. We focused the model evaluation on regional performance in rural areas for two reasons: (1) the relatively coarse grid inadequately resolves details in urban chemistry related to primary precursor emissions, and (2) this study focuses on updates to model chemistry and processes largely affecting secondary pollutants (ozone, aged NOx, organic and inorganic aerosols) that are generated downwind of their precursor sources and dispersed over regional scales. IMPROVE, CASTNet and NADP sites are located in rural areas. We extracted hourly ozone data from AQS sites characterized as "RURAL", but filtering out those with landuse categorized as "COMMERCIAL", "INDUSTRIAL", and "RESIDENTIAL". Ozone performance metrics were determined for hourly ozone (with and without a cutoff of 40 ppb), and for MDA8 ozone with no cutoff. In future reports addressing PM, our evaluation will focus on speciated $PM_{2.5}$ rather than total $PM_{2.5}$ mass to identify specific impacts to individual PM components and mass budgets stemming from the model updates. We will specifically address sulfate, nitrate, ammonium, elemental carbon and total organic mass (not organic carbon mass). However, we ignore primary "other" $PM_{2.5}$ and coarse PM as both are dominated by dust sources and not impacted by model updates developed in this project.

The modeling domain was separated into nine performance regions (Figure 3). Ozone (and later PM and wet deposition) statistics were calculated for all sites and all networks in each region. To specifically address effects from the CB6r4 halogen update in Task 7, we focus our evaluation on just hourly ozone performance at AQS monitors throughout the CONUS domain and at specific monitors along the Gulf of Mexico and southern Atlantic coastlines. PM and wet deposition performance comparisons will be conducted in later Tasks.

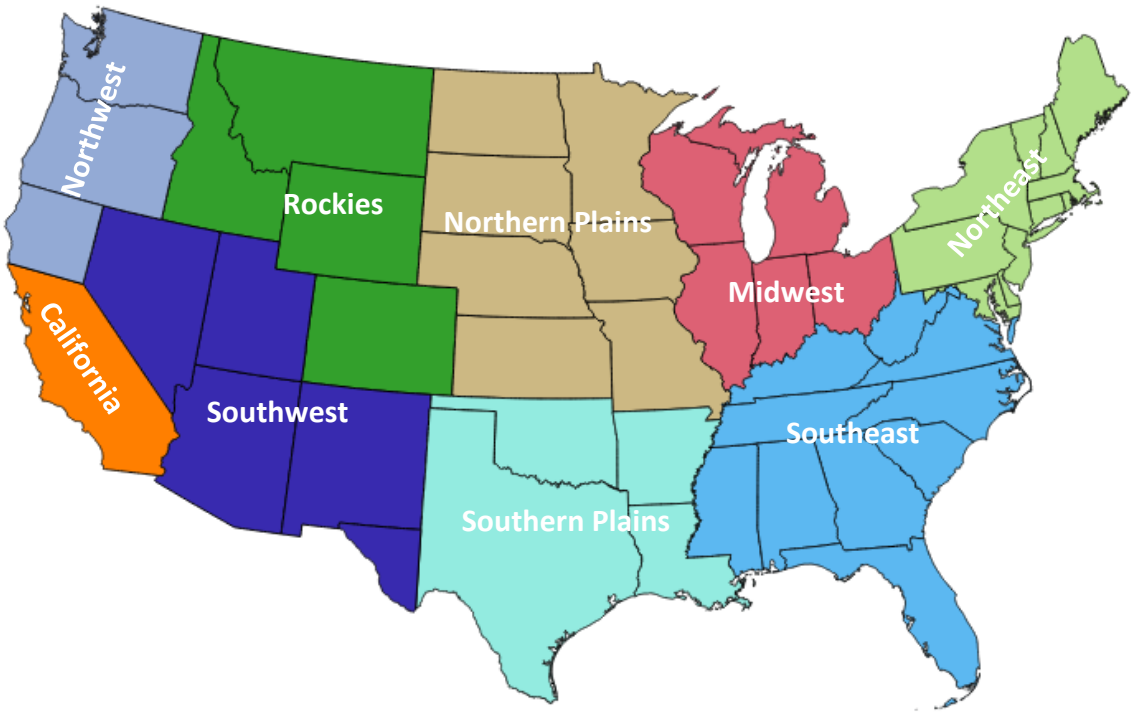


**Figure 3. Breakdown of the US into nine model performance evaluation regions.**

## Results

Figure 4 displays a map of normalized mean bias (NMB) over July 2011 at each AQS monitoring site across the CONUS domain for hourly ozone with a 40 ppb cutoff applied. Results for the CB6r2 and CB6r4 cases are shown. Figure 5 shows similar maps for normalized mean error (NME). Table 1 lists these metrics and correlation by performance region (Figure 3) for both cases. Ozone statistics for CB6r2 and CB6r4 are very similar and typical of recent regional photochemical modeling applications. Ozone is over predicted in the eastern US and especially over the southeast region. Ozone in the central, intermountain and northwest portions of the US tends to be well simulated, whereas ozone is under predicted in California and Arizona. Generally, CB6r4 results in slightly lower ozone nationwide, improving over predictions but degrading performance in the two under predicted regions. The Southern Plains and Southeast regions, where ozone over the Gulf and Atlantic coastlines is most influential, exhibit the greatest statistical improvements.

Figure 6 shows similar ozone performance maps for eight sites along the Gulf of Mexico and Southern Atlantic coastlines. Our statistical analyses for this region address all hourly ozone predictions and observation pairings without applying cutoffs because a majority of measured ozone transported onshore is typically below 40 ppb. Extremely large bias and error occur at

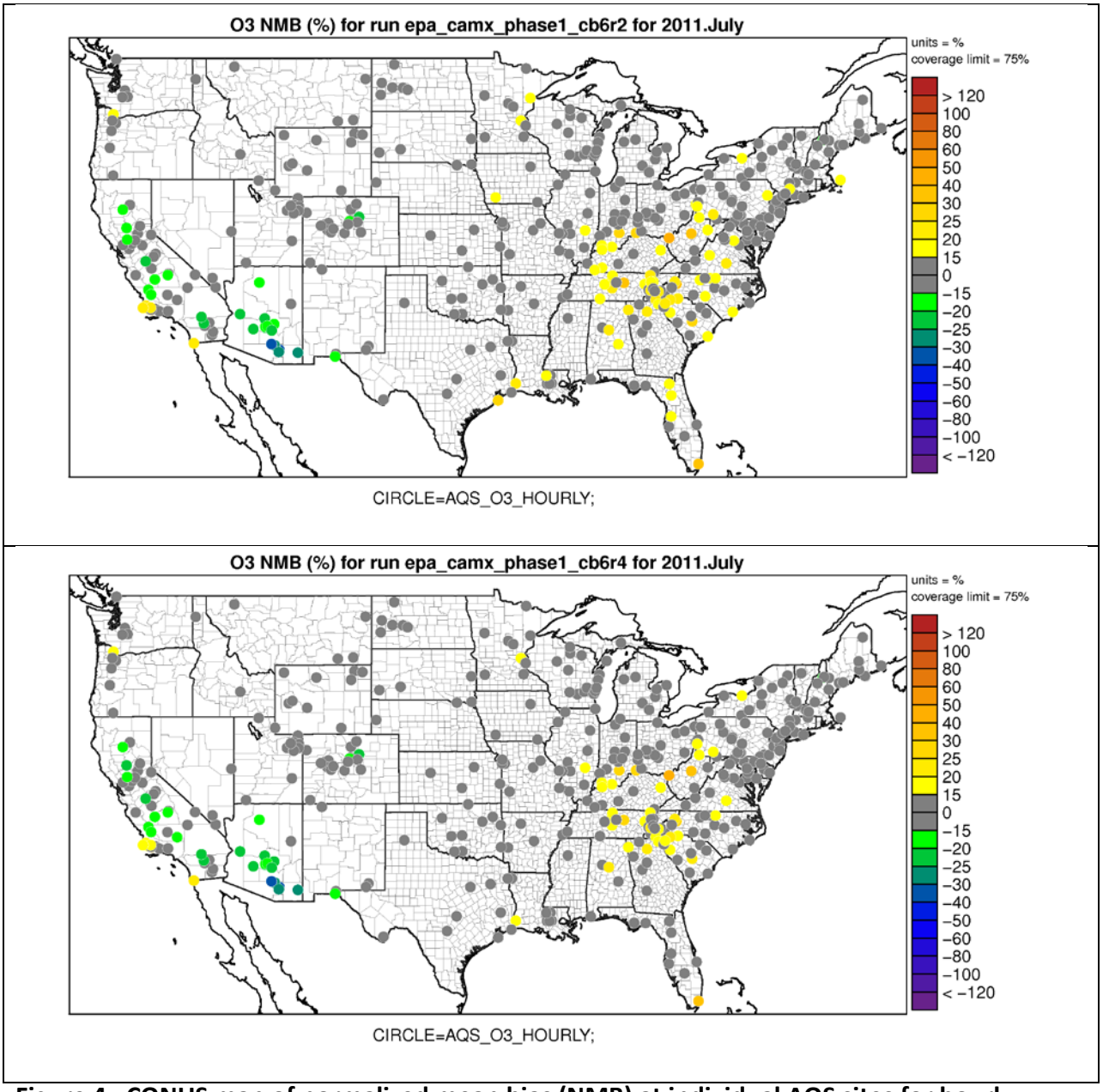


**Figure 4. CONUS map of normalized mean bias (NMB) at individual AQS sites for hourly ozone with a 40 ppb cutoff applied: CB6r2 (top) and CB6r4 (bottom).**

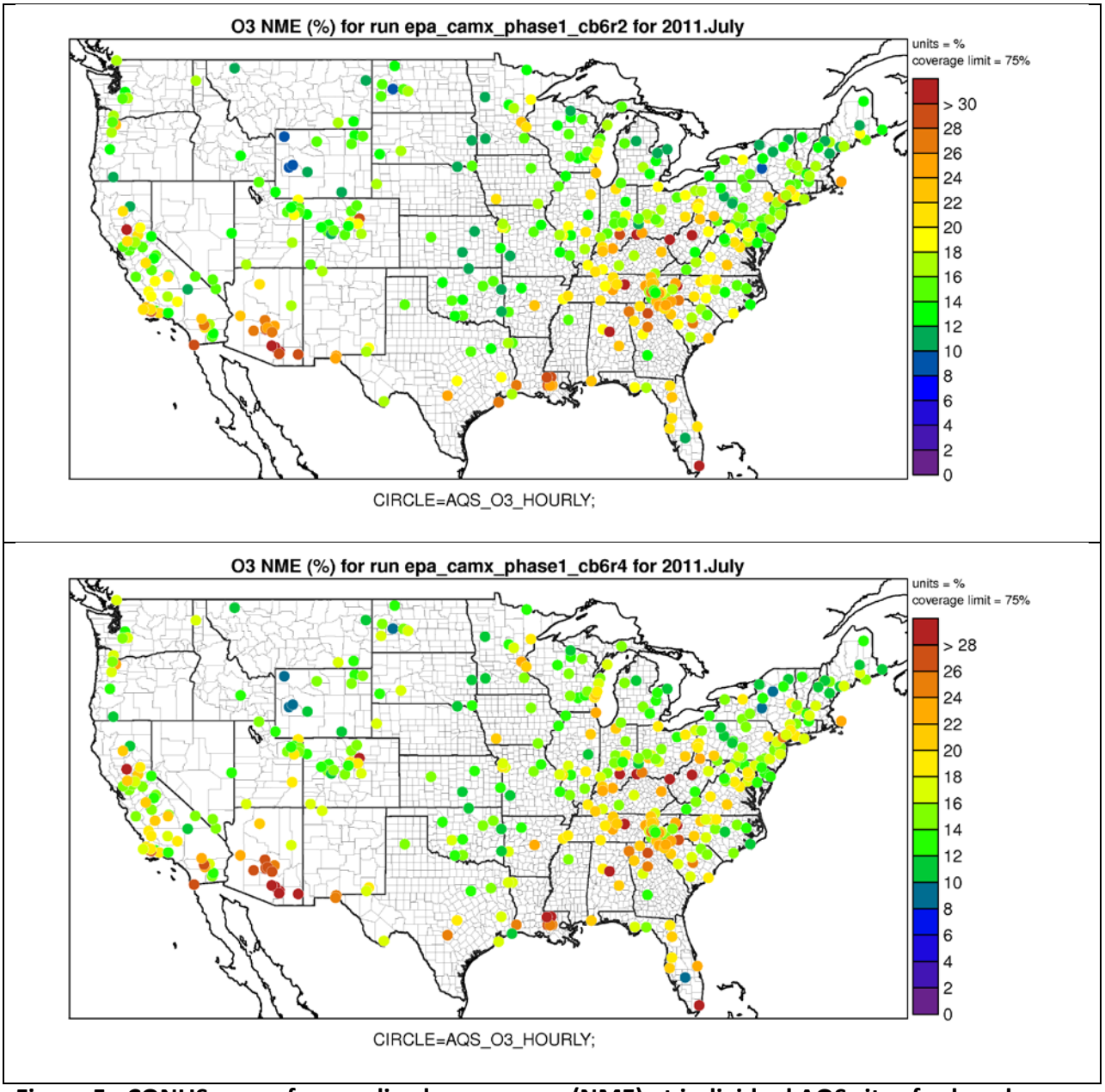


**Figure 5. CONUS map of normalized mean error (NME) at individual AQS sites for hourly ozone with a 40 ppb cutoff applied: CB6r2 (top) and CB6r4 (bottom).**

**Table 1. Regional NMB (%), NME (%) and correlation (R, decimal) statistics for hourly ozone with a 40 ppb cutoff applied in the CB6r2 and CB6r4 cases. NMB and NME values outside of EPA statistical benchmarks (±15% and 35%, respectively) are shown in red. Changes from CB6r2 to CB6r4 are shown in red for degraded performance and green for improved performance.**

| | NMB (%) | | | NME (%) | | | R | | |
|---|---|---|---|---|---|---|---|---|---|
| Region | CB6r2 | CB6r4 | Change | CB6r2 | CB6r4 | Change | CB6r2 | CB6r4 | Change |
| Northwest | 2.3 | 1.6 | -0.7 | 13.2 | 13.2 | 0 | 0.90 | 0.90 | 0 |
| California | -2.6 | -3.7 | -1.1 | 16.9 | 16.7 | -0.2 | 0.75 | 0.77 | +0.02 |
| Rockies | 1.0 | 0.6 | -0.4 | 11.1 | 11.1 | 0 | 0.71 | 0.71 | 0 |
| Southwest | -8.5 | -9.1 | -0.6 | 16.0 | 16.3 | +0.3 | 0.51 | 0.50 | -0.01 |
| Northern Plains | 9.2 | 8.0 | -1.2 | 15.6 | 15.2 | -0.4 | 0.73 | 0.72 | -0.01 |
| Southern Plains | 8.6 | 6.2 | -2.4 | 18.7 | 17.8 | -0.9 | 0.68 | 0.70 | +0.02 |
| Midwest | 10.5 | 9.2 | -1.3 | 15.6 | 14.9 | -0.7 | 0.74 | 0.74 | 0 |
| Southeast | 21.3 | 18.9 | -2.4 | 23.7 | 21.8 | -1.9 | 0.74 | 0.74 | 0 |
| Northeast | 8.9 | 7.4 | -1.5 | 14.4 | 13.6 | -0.8 | 0.85 | 0.85 | 0 |

these coastal sites. Only marginal differences in ozone NMB and NME are apparent between the CB6r2 and CB6r4 cases.

We have separated our coastal ozone analyses into four sites located on the Gulf of Mexico coast and four sites on the Southern Atlantic coast. Figures 7 and 8 show scatter and soccer goal plots, respectively, for all ozone hours at the Gulf of Mexico sites. The largest over prediction occurs at the Galveston, TX site (481671034). CB6r4 results in some reduction in ozone over predictions by roughly 10 percentage points overall. Figures 9 and 10 show the same plots for the Southern Atlantic sites. Over predictions tend to be smaller than the Gulf of Mexico, and CB6r4 results in roughly a 5 percentage point improvement overall.

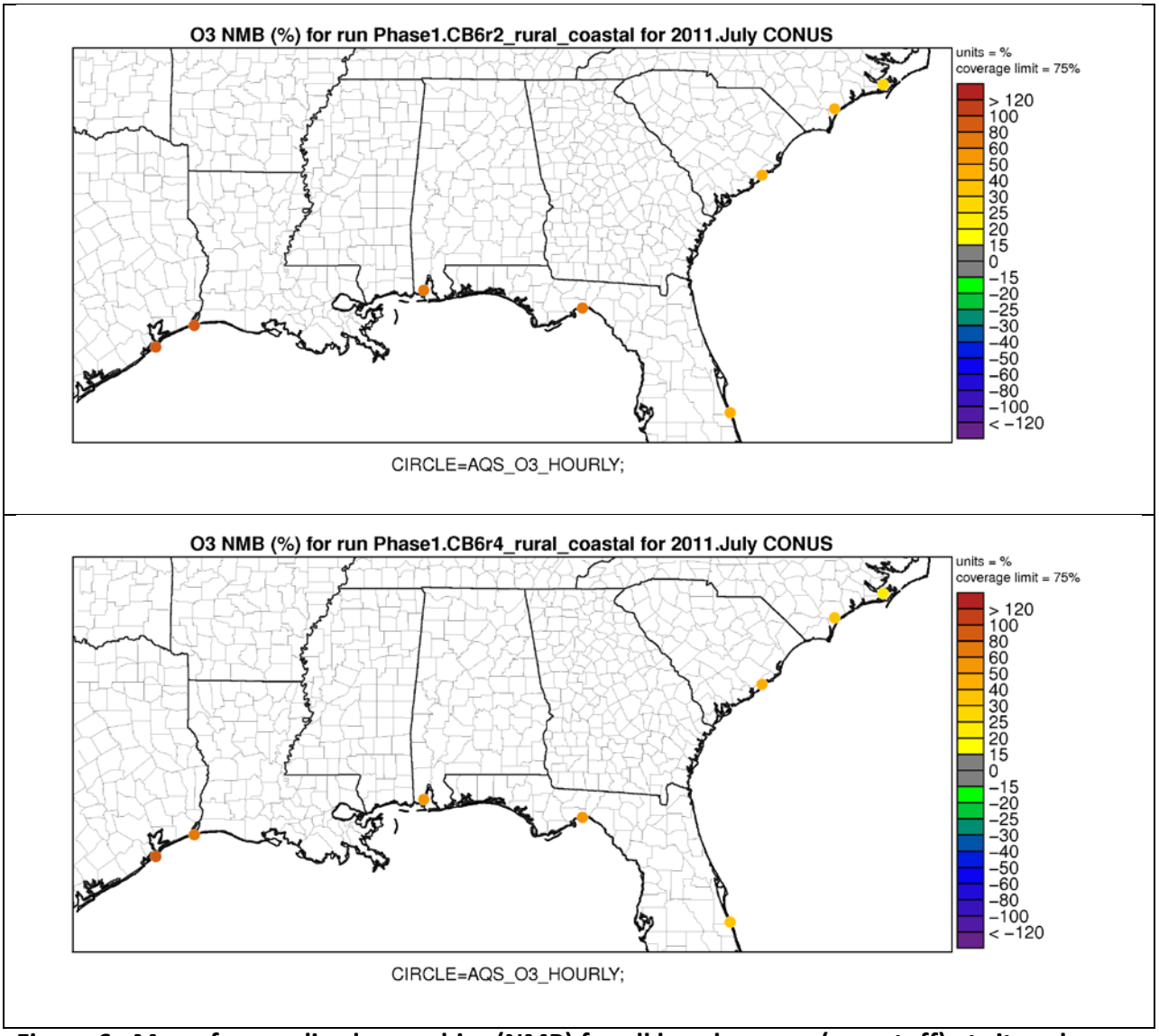


**Figure 6. Map of normalized mean bias (NMB) for all hourly ozone (no cutoff) at sites along the Gulf of Mexico and Southern Atlantic coastlines: CB6r2 (top) and CB6r4 (bottom).**

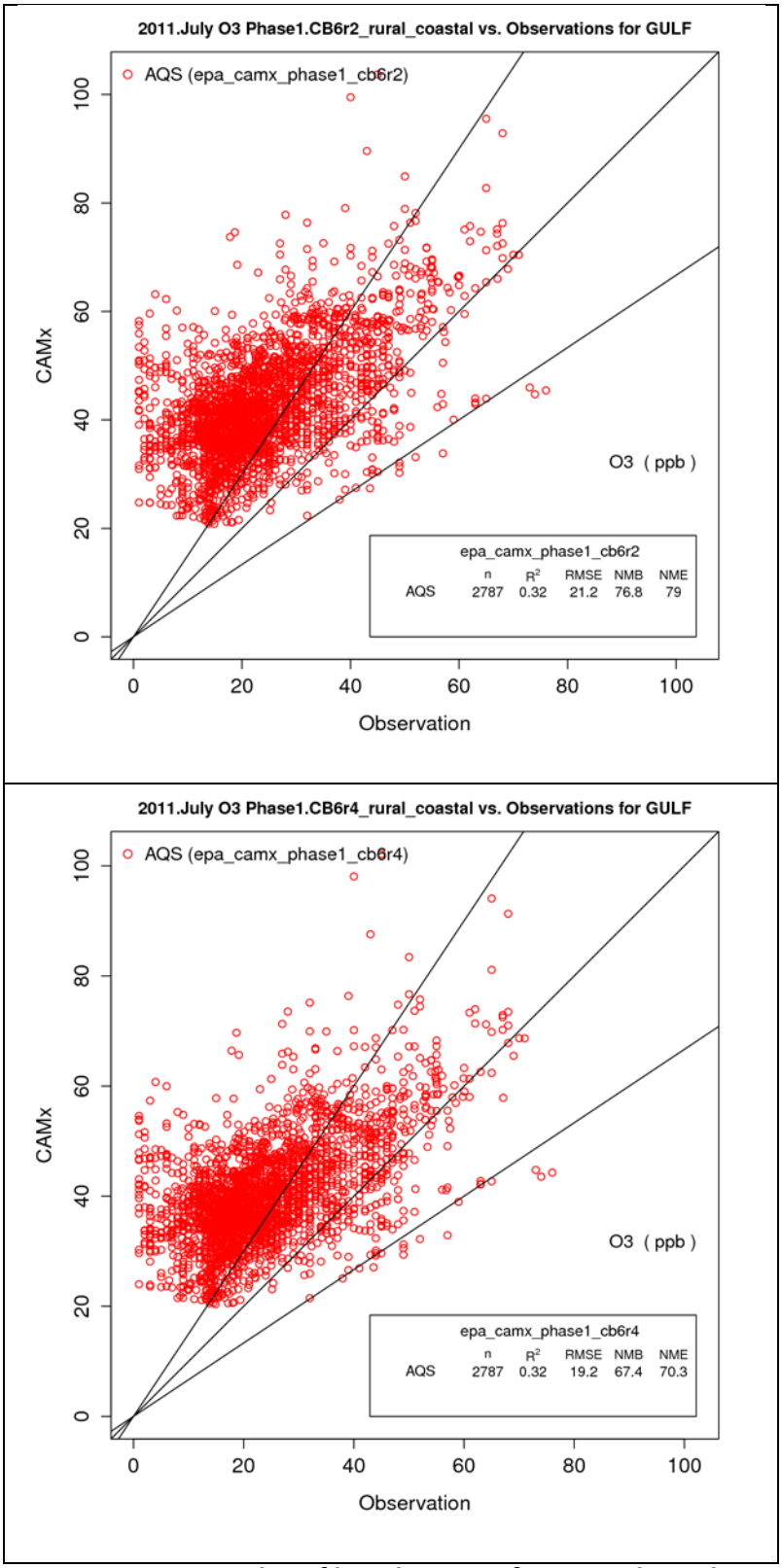


**Figure 7. Scatter plot of hourly ozone for sites along the Gulf of Mexico coastline: CB6r2 (top) and CB6r4 (bottom).**

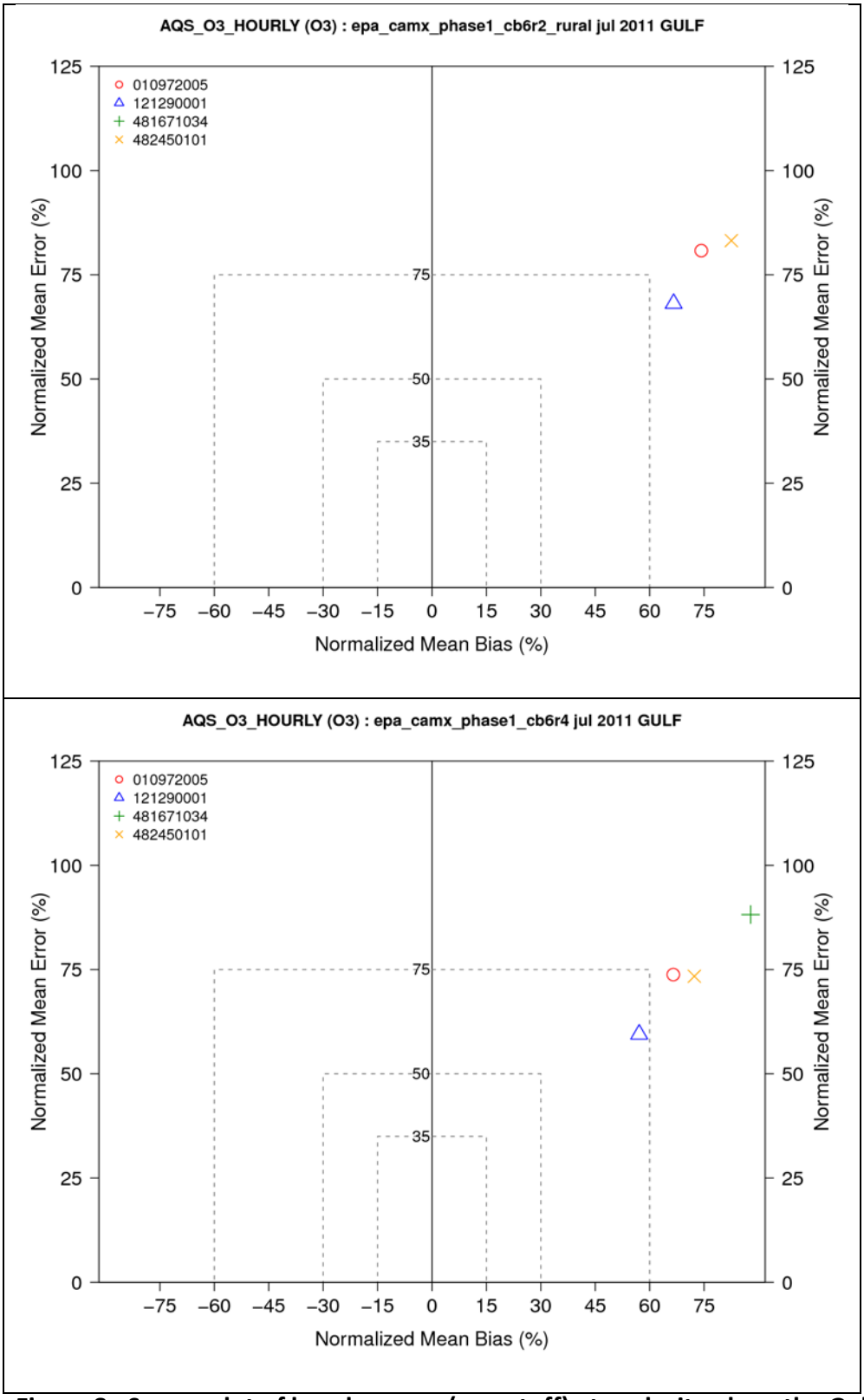


**Figure 8. Soccer plot of hourly ozone (no cutoff) at each site along the Gulf of Mexico coastline: CB6r2 (top) and CB6r4 (bottom). The data point for site 481671034 is outside the plot bounds of the upper chart.**

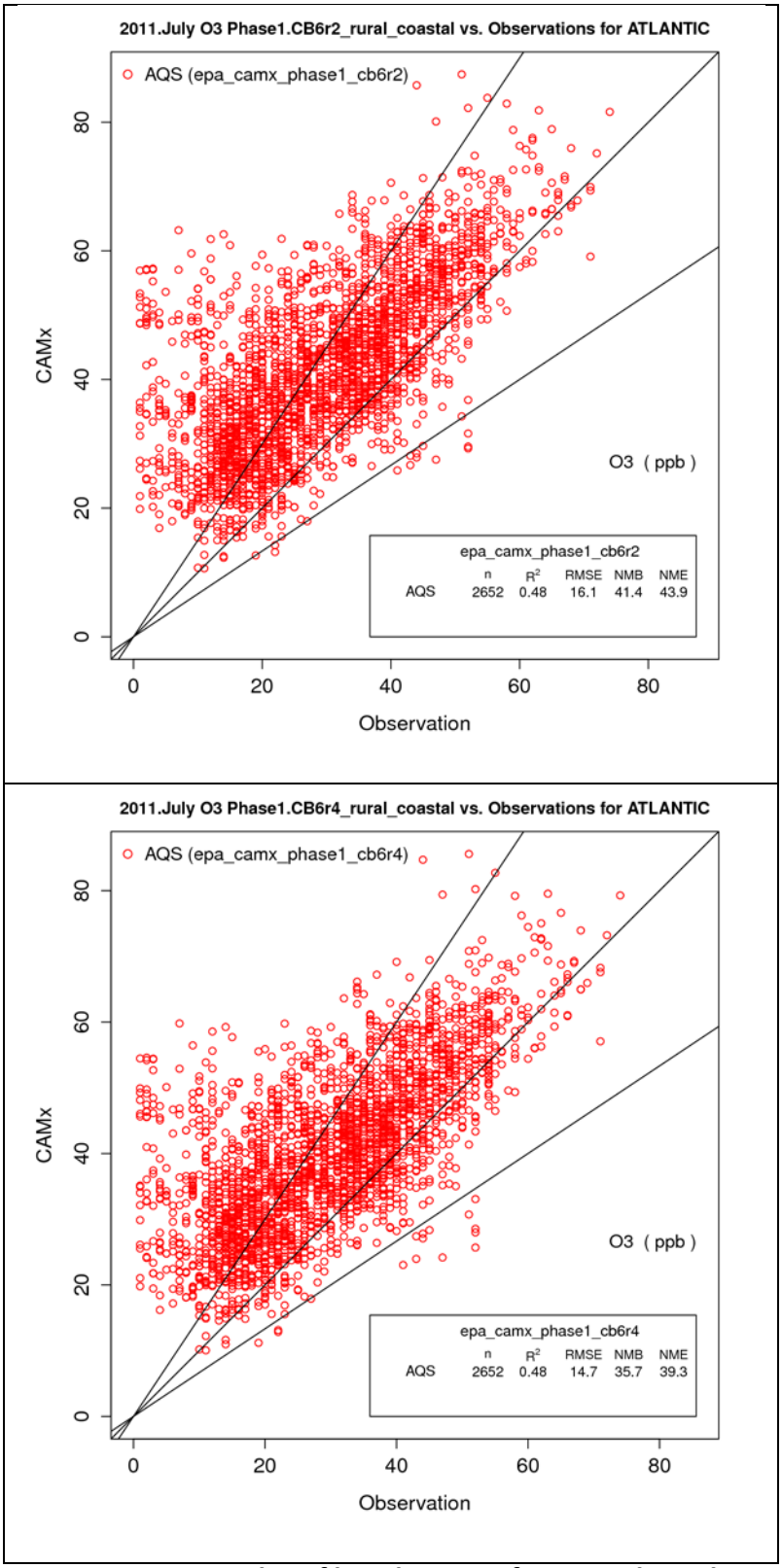


**Figure 9. Scatter plot of hourly ozone for sites along the Southern Atlantic coastline: CB6r2 (top) and CB6r4 (bottom).**

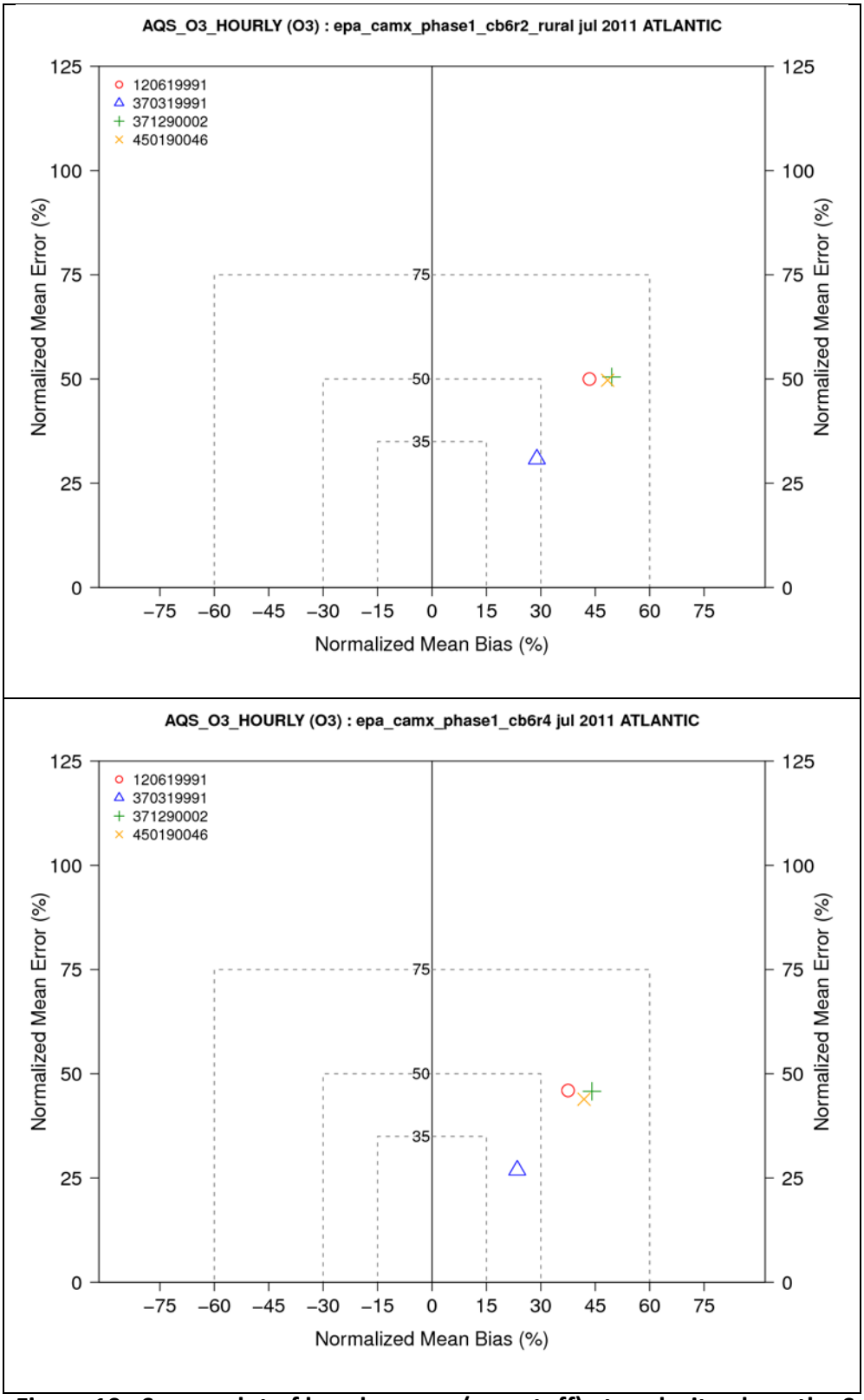


**Figure 10. Soccer plot of hourly ozone (no cutoff) at each site along the Southern Atlantic coastline: CB6r2 (top) and CB6r4 (bottom).**

## User Instructions

RE is delivering an interim version of CAMx (v6.32) to EPA with this report. CAMx v6.32 will not be publicly distributed but will be incorporated into the next public release (v6.40) along with all other CAMx updates from this Work Assignment after completion of all tasks. RE will work with EPA's CMAQ developers to install CB6r4 into CMAQ.

CAMx v6.32 includes the following updates over the previous public release (v6.30):

- CB6r4 with a specialized halogen reaction solver as Mechanism 4; CB6r2h remains as Mechanism 3;
- SA update for ozone depletion by Ix and impacts to the nitrogen tracer class;
- In-line Ix emissions (can be used with either CB6r4 or CB6r2h) – hourly estimates of $I_2$ and HOI emission rates are output to the deposition output files for diagnostic purposes;
- An update that exploits the CAMx input landuse file's ability to differentiate between fresh and ocean/salt water bodies.

The list below presents a few basic user instructions on using CAMx v6.32 with CB6r4:

- Compile CAMx as you normally would using the "Makefile" provided with the source code.
- Specify the path to the CB6r4 (Mechanism 4) chemistry parameters file in the CAMx namelist control file (a Mechanism 4 chemistry parameters file is provided with the source code).
- Add a new namelist flag "`Inline_Ix_Emissions`" to the CAMx namelist control file, set it to "`.TRUE.`" This eliminates the need to supply oceanic Ix emissions in your input gridded emissions files. If Ix (i.e., $I_2$ and/or HOI) emissions are present on your input files, CAMx will stop with an error to avoid double-counting. If in-line emissions are not invoked, you may continue to use externally-derived halogen emissions from the SEASALT pre-processor.
- Convert CAMx input landuse files to differentiate between fresh and ocean/salt water bodies, as further described below (converted landuse files for the 2011 12 km CONUS domain will be provided to the EPA).

### Converting Landuse Files

The CAMx input landuse file lists the fractional coverage of 26 land cover types per grid cell according to the scheme used by the Zhang dry deposition algorithm. These land cover types include "WATER" (index = 1) and "LAKE" (index=3). Since none of the land cover datasets employed by meteorological models (WRF, MM5, RAMS) differentiate between fresh and ocean water bodies, the respective CAMx meteorological interface programs populate only the "WATER" classification for any water type. Now that the new in-line Ix emissions algorithm is applied only for ocean water bodies, a differentiation between fresh and ocean water is needed. This capability extends to both Zhang and Wesely landuse options within CAMx.

A new program called "watermask" converts existing CAMx landuse files to make this distinction. The program is run twice: (1) read an existing landuse file and develop a text-based water map that shows all grid cells containing some fraction of water in each grid cell, which must then be edited to remove fresh water cells; and (2) read the edited water map and convert the existing landuse file to populate the "WATER" category with ocean fractions and the "LAKE" category with fresh water fractions.

The intermediate water map file contains an array of single characters denoting cells containing any water. Cells containing <5% water are blank; cells containing water fractions are noted with integers ranging from "1" (5-15%) to "9" (85-95%) and as "X" for fractions >95%. The array is arranged like a map to ease visual navigation, with northernmost rows at the top and southernmost rows at the bottom, west to the left and east to the right. The water map file is a readable text format and it has the following structure:

```
Text, ny, nx                        (A20,2i10)
Loop from j = ny grid rows to 1
   (water(i,j),i=1,nx)              (999A1)
End loop
```

where the variables have the following definitions:

| | |
|---|---|
| `text` | Text identifying file |
| `nx` | Number of grid columns |
| `ny` | Number of grid rows |
| `water` | Single-character water index for row `j` and column `i` |

Figure 11 shows an example of a small single-grid water map file.

This file initially makes no distinction whether water cells are ocean or fresh water. It is up to the user to edit each array and replace fresh water cells with blank (" "), which admittedly can be difficult and tedious for large grids or areas with combinations of complex coastlines and inland water bodies. GIS software could be used to ease this process. Then each modified water map is used to convert an input landuse file. Generally, the definition of ocean water bodies does not change in time, and so a single water map file can be used to convert multiple landuse files. However, for domains including time-varying sea ice cover, a single "ice-free" water mask should be developed so that daily water maps do not need to be generated and edited as the ice cover evolves.

```
Water map file              64        10
XXXXXX5                  2           1    9   78     1XXXXXXXXX
XXXXXX3             6                1    8         8XXXXXXXXXX
XXXXXXX1 1 2            1      1       1    111     4XXXXXXXXXXX
XXXXXXX811                        1     1111        7XXXXXXXXXXX
XXXXXXXX5 1                            1            9XXXXXXXXXXX
XXXXXXXXX4                              1          6XXXXXXXXXXXX
XXXXXXXXXXX2  6                  263598761876554   3XXXXXXXXXXXXX
XXXXXXXXXXX6  37                 4XXXXXXXXX9XXXXX5  3XXXXXXXXXXXXX
XXXXXXXXXXXX1 45                6XXXXXXXXXXXXXXXXX8  2XXXXXXXXXXXX
XXXXXXXXXXXX8  67                4XXXXXXXXXXXXXXXXXX2 1XXXXXXXXXXXX

Water map file              64        10
XXXXXX5                                             1XXXXXXXXX
XXXXXX3                                            8XXXXXXXXXX
XXXXXXX1                                           4XXXXXXXXXXX
XXXXXXX8                                           7XXXXXXXXXXX
XXXXXXXX5                                          9XXXXXXXXXXX
XXXXXXXXX4                                        6XXXXXXXXXXXX
XXXXXXXXXX2  6                  26359876 876554   3XXXXXXXXXXXXX
XXXXXXXXXX6  37                 4XXXXXXXXX9XXXXX5  3XXXXXXXXXXXXX
XXXXXXXXXXX1 45                6XXXXXXXXXXXXXXXXX8  2XXXXXXXXXXXX
XXXXXXXXXXX8  67                4XXXXXXXXXXXXXXXXXX2 1XXXXXXXXXXXX
```

**Figure 11. Example structure of a water map file generated and used by the "watermask" program to convert CAMx input landuse files that differentiate ocean and fresh water bodies. Top panel shows an initial water map file with all water body fractions, including oceans, lakes and rivers. The bottom panel shows the same file edited to remove non-ocean water fractions.**

## References


Atkinson, R., W.P. Carter, A.M. Winer. 1983. Effects of temperature and pressure on alkyl nitrate yields in the nitrogen oxide (NOx) photooxidations of n-pentane and n-heptane. *Journal of Physical Chemistry*, 87(11), 2012-2018.

Carpenter, L.J. 2003. Iodine in the marine boundary layer. *Chemical Reviews*, 103, 4953-4962.

Carpenter, L.J., S.M. MacDonald, M.D. Shaw, R. Kumar, R.W. Saunders, R. Parthipan, J. Wilson, J.M.C. Plane. 2013. Atmospheric iodine levels influenced by sea surface emissions of inorganic iodine. *Nature Geoscience*, 6, no. 2: 108-111.

Carter, W.P. and G. Heo. 2013. Development of revised SAPRC aromatics mechanisms. *Atmospheric Environment*, 77, 404-414.

Chameides, W.L., and D.D. Davis. 1980. Iodine: Its Possible Role in Tropospheric Photochemistry. *J. Geophys. Res.*, 85, 7383–7398, doi:10.1029/JC085iC12p07383.

Emery, C., J. Jung, B. Koo, G. Yarwood. 2015. Improvements to CAMx Snow Cover Treatments and Carbon Bond Chemical Mechanism for Winter Ozone. Prepared for the Utah Department of Environmental Quality, Division of Air Quality, Salt Lake City, UT. Prepared by Ramboll Environ, Novato, CA (August 2015).

Emery, C., Z. Liu, B. Koo, G. Yarwood. 2016. Improved Halogen Chemistry for CAMx Modeling. Prepared for the Texas Commission on Environmental Quality, Austin, TX. Prepared by Ramboll Environ, Novato, CA (May 2016).

Fisher, J.A., Jacob, D.J., Travis, K.R., Kim, P.S., Marais, E.A., Chan Miller, C., Yu, K., Zhu, L., Yantosca, R.M., Sulprizio, M.P., Mao, J., Wennberg, P.O., Crounse, J.D., Teng, A.P., Nguyen, T.B., St. Clair, J.M., Cohen, R.C., Romer, P., Nault, B.A., Wooldridge, P.J., Jimenez, J.L., Campuzano-Jost, P., Day, D.A., Hu, W., Shepson, P.B., Xiong, F., Blake, D.R., Goldstein, A.H., Misztal, P.K., Hanisco, T.F., Wolfe, G.M., Ryerson, T.B., Wisthaler, A., Mikoviny, T. 2016. Organic nitrate chemistry and its implications for nitrogen budgets in an isoprene- and monoterpene-rich atmosphere: constraints from aircraft (SEAC4RS) and ground-based (SOAS) observations in the Southeast US. *Atmos. Chem. Phys.*, 16, 5969-5991, doi:10.5194/acp-16-5969-2016.

Garland, J. A., and H. Curtis. 1981. Emission of iodine from the sea surface in the presence of ozone. *Journal of Geophysical Research: Oceans* (1978–2012), 86, no. C4: 3183-3186.

Goliff, W.S., W.R. Stockwell, C.V. Lawson. 2013. The regional atmospheric chemistry mechanism, version 2. *Atmospheric Environment*, 68, 174-185.

Hertel, O., R. Berkowicz, J. Christensen, J., Ø. Hov. 1993. Test of two numerical schemes for use in atmospheric transport-chemistry models. *Atmospheric Environment, Part A, General Topics*, 27(16), 2591-2611.

Hildebrandt Ruiz, L. and G. Yarwood. 2013. Interactions between Organic Aerosol and NOy: Influence on Oxidant Production. Final report for AQRP project 12-012. Available at http://aqrp.ceer.utexas.edu/projectinfoFY12_13%5C12-012%5C12-012%20Final%20Report.pdf.

Jacobs, M.I., Burke, W.J., Elrod, M.J. 2014. Kinetics of the reactions of isoprene-derived hydroxynitrates: gas phase epoxide formation and solution phase hydrolysis. *Atmos. Chem. Phys.*, 14, 8933-8946, doi:10.5194/acp-14-8933-2014.

Lee, L., P.J. Wooldridge, J.B. Gilman, C. Warneke, J. de Gouw, R.C. Cohen. 2014. Low temperatures enhance organic nitrate formation: evidence from observations in the 2012 Uintah Basin Winter Ozone Study. *Atmospheric Chemistry and Physics Discussions*, 14(11), 17401-17438.

Mahajan, A.S., H. Oetjen, A. Saiz-Lopez, J.D. Lee, G.B. McFiggans, J.M.C. Plane. 2009. Reactive iodine species in a semi-polluted environment. *Geophys. Res. Lett.*, 36, L16803, doi:10.1029/2009GL038018.

Mahajan, A.S., J.M.C. Plane, H. Oetjen, L. Mendes, R.W. Saunders, A. Saiz-Lopez, C.E. Jones, L.J. Carpenter, G.B. McFiggans. 2010. Measurement and modelling of tropospheric reactive halogen species over the tropical Atlantic Ocean. *Atmos. Chem. Phys.*, 10, 4611-4624, 2010 doi:10.5194/acp-10-4611-2010.

Perring, A.E., S.E. Pusede, R.C. Cohen. 2013. An observational perspective on the atmospheric impacts of alkyl and multifunctional nitrates on ozone and secondary organic aerosol. *Chemical Reviews*, 113(8), 5848-5870.

Prados-Roman, C., C.A. Cuevas, R.P. Fernandez, D.E. Kinnison, J.F. Lamarque, A. Saiz-Lopez. 2015. A negative feedback between anthropogenic ozone pollution and enhanced ocean emissions of iodine. *Atmospheric Chemistry and Physics*, 15(4), 2215-2224.

Ramboll Environ. 2016. User's Guide: Comprehensive Air Quality Model with Extensions, Version 6.30. Prepared by Ramboll Environ, Novato, CA (March 2016). www.camx.com.

Rollins, A.W., Pusede, S., Wooldridge, P., Min, K.-E., Gentner, D.R., Goldstein, A.H., Liu, S., Day, D.A., Russell, L.M., Rubitschun, C.L., Surratt, J.D., Cohen, R.C. 2013. Gas/particle partitioning of total alkyl nitrates observed with TD-LIF in Bakersfield. *J. Geophys. Res. Atmos.*, 118, 6651–6662, doi:10.1002/jgrd.50522.

Saunders, S.M., M.E. Jenkin, R.G. Derwent, M.J. Pilling. 2003. Protocol for the development of the Master Chemical Mechanism, MCM v3 (Part A): tropospheric degradation of non-aromatic volatile organic compounds. *Atmospheric Chemistry and Physics*, 3(1), 161-180.

Whitten, G.Z., G. Heo, Y. Kimura, E. McDonald-Buller, D.T. Allen, W.P. Carter, G. Yarwood. 2010. A new condensed toluene mechanism for Carbon Bond: CB05-TU. *Atmospheric Environment*, 44(40), 5346-5355.

Yarwood, G., J. Jung, U. Nopmongcol, C. Emery. 2012. Improving CAMx Performance in Simulating Ozone Transport from the Gulf of Mexico. Final Report for Work Order No. 582-11-10365-FY12-05.

Yarwood, G., T. Sakulyanontvittaya, U. Nopmongcol, B. Koo. 2014. Ozone Depletion by Bromine and Iodine over the Gulf of Mexico. Final Report for Work Order No. 582-11-10365-FY14-12 https://www.tceq.texas.gov/airquality/airmod/project/pj_report_pm.html.

Yeh, G.K. and P.J. Ziemann. 2014. Alkyl Nitrate Formation from the Reactions of C8–C14 n-Alkanes with OH Radicals in the Presence of NO x: Measured Yields with Essential Corrections for Gas–Wall Partitioning. *The Journal of Physical Chemistry*, A, 118 (38), 8797-8806.

# Appendix A: CB6r4 Mechanism Listing

**Table A-1. Reactions and rate constant expressions for the CB6r4 mechanism. $k_{298}$ is the rate constant at 298 K and 1 atmosphere using units in molecules/cm$^3$ and 1/s. For photolysis reactions $k_{298}$ shows the photolysis rate at a solar zenith angle of 60° and height of 600 m MSL/AGL.**

| Number | Reactants and Products | Rate Constant Expression | $k_{298}$ |
|---|---|---|---|
| 1 | NO2 = NO + O | Photolysis | 6.30E-3 |
| 2 | O + O2 + M = O3 + M | k = 5.68E-34 (T/300)^-2.6 | 5.78E-34 |
| 3 | O3 + NO = NO2 | k = 1.40E-12 exp(-1310/T) | 1.73E-14 |
| 4 | O + NO + M = NO2 + M | k = 1.00E-31 (T/300)^-1.6 | 1.01E-31 |
| 5 | O + NO2 = NO | k = 5.50E-12 exp(188/T) | 1.03E-11 |
| 6 | O + NO2 = NO3 | Falloff: F=0.6; n=1<br>k(0) = 1.30E-31 (T/300)^-1.5<br>k(inf) = 2.30E-11 (T/300)^0.24 | 2.11E-12 |
| 7 | O + O3 = | k = 8.00E-12 exp(-2060/T) | 7.96E-15 |
| 8 | O3 = O | Photolysis | 3.33E-4 |
| 9 | O3 = O1D | Photolysis | 8.78E-6 |
| 10 | O1D + M = O + M | k = 2.23E-11 exp(115/T) | 3.28E-11 |
| 11 | O1D + H2O = 2 OH | k = 2.14E-10 | 2.14E-10 |
| 12 | O3 + OH = HO2 | k = 1.70E-12 exp(-940/T) | 7.25E-14 |
| 13 | O3 + HO2 = OH | k = 2.03E-16 (T/300)^4.57 exp(693/T) | 2.01E-15 |
| 14 | OH + O = HO2 | k = 2.40E-11 exp(110/T) | 3.47E-11 |
| 15 | HO2 + O = OH | k = 2.70E-11 exp(224/T) | 5.73E-11 |
| 16 | OH + OH = O | k = 6.20E-14 (T/298)^2.6 exp(945/T) | 1.48E-12 |
| 17 | OH + OH = H2O2 | Falloff: F=0.5; n=1.13<br>k(0) = 6.90E-31 (T/300)^-0.8<br>k(inf) = 2.60E-11 | 5.25E-12 |
| 18 | OH + HO2 = | k = 4.80E-11 exp(250/T) | 1.11E-10 |
| 19 | HO2 + HO2 = H2O2 | k = k1 + k2 [M]<br>k1 = 2.20E-13 exp(600/T)<br>k2 = 1.90E-33 exp(980/T) | 2.90E-12 |
| 20 | HO2 + HO2 + H2O = H2O2 | k = k1 + k2 [M]<br>k1 = 3.08E-34 exp(2800/T)<br>k2 = 2.66E-54 exp(3180/T) | 6.53E-30 |
| 21 | H2O2 = 2 OH | Photolysis | 3.78E-6 |
| 22 | H2O2 + OH = HO2 | k = 2.90E-12 exp(-160/T) | 1.70E-12 |
| 23 | H2O2 + O = OH + HO2 | k = 1.40E-12 exp(-2000/T) | 1.70E-15 |
| 24 | NO + NO + O2 = 2 NO2 | k = 3.30E-39 exp(530/T) | 1.95E-38 |
| 25 | HO2 + NO = OH + NO2 | k = 3.45E-12 exp(270/T) | 8.54E-12 |
| 26 | NO2 + O3 = NO3 | k = 1.40E-13 exp(-2470/T) | 3.52E-17 |
| 27 | NO3 = NO2 + O | Photolysis | 1.56E-1 |
| 28 | NO3 = NO | Photolysis | 1.98E-2 |
| 29 | NO3 + NO = 2 NO2 | k = 1.80E-11 exp(110/T) | 2.60E-11 |
| 30 | NO3 + NO2 = NO + NO2 | k = 4.50E-14 exp(-1260/T) | 6.56E-16 |
| 31 | NO3 + O = NO2 | k = 1.70E-11 | 1.70E-11 |
| 32 | NO3 + OH = HO2 + NO2 | k = 2.00E-11 | 2.00E-11 |
| 33 | NO3 + HO2 = OH + NO2 | k = 4.00E-12 | 4.00E-12 |
| 34 | NO3 + O3 = NO2 | k = 1.00E-17 | 1.00E-17 |
| 35 | NO3 + NO3 = 2 NO2 | k = 8.50E-13 exp(-2450/T) | 2.28E-16 |

| Number | Reactants and Products | Rate Constant Expression | $k_{298}$ |
|---|---|---|---|
| 36 | NO3 + NO2 = N2O5 | Falloff: F=0.35; n=1.33<br>k(0) = 3.60E-30 (T/300)^-4.1<br>k(inf) = 1.90E-12 (T/300)^0.2 | 1.24E-12 |
| 37 | N2O5 = NO3 + NO2 | Falloff: F=0.35; n=1.33<br>k(0) = 1.30E-3 (T/300)^-3.5 exp(-11000/T)<br>k(inf) = 9.70E+14 (T/300)^0.1 exp(-11080/T) | 4.46E-2 |
| 38 | N2O5 = NO2 + NO3 | Photolysis | 2.52E-5 |
| 39 | N2O5 + H2O = 2 HNO3 | k = 1.00E-22 | 1.00E-22 |
| 40 | NO + OH = HONO | Falloff: F=0.81; n=0.87<br>k(0) = 7.40E-31 (T/300)^-2.4<br>k(inf) = 3.30E-11 (T/300)^-0.3 | 9.77E-12 |
| 41 | NO + NO2 + H2O = 2 HONO | k = 5.00E-40 | 5.00E-40 |
| 42 | HONO + HONO = NO + NO2 | k = 1.00E-20 | 1.00E-20 |
| 43 | HONO = NO + OH | Photolysis | 1.04E-3 |
| 44 | HONO + OH = NO2 | k = 2.50E-12 exp(260/T) | 5.98E-12 |
| 45 | NO2 + OH = HNO3 | Falloff: F=0.6; n=1<br>k(0) = 1.80E-30 (T/300)^-3<br>k(inf) = 2.80E-11 | 1.06E-11 |
| 46 | HNO3 + OH = NO3 | k = k1 + k3 [M] / (1 + k3 [M] / k2)<br>k1 = 2.40E-14 exp(460/T)<br>k2 = 2.70E-17 exp(2199/T)<br>k3 = 6.50E-34 exp(1335/T) | 1.54E-13 |
| 47 | HNO3 = OH + NO2 | Photolysis | 2.54E-7 |
| 48 | HO2 + NO2 = PNA | Falloff: F=0.6; n=1<br>k(0) = 1.80E-31 (T/300)^-3.2<br>k(inf) = 4.70E-12 | 1.38E-12 |
| 49 | PNA = HO2 + NO2 | Falloff: F=0.6; n=1<br>k(0) = 4.10E-5 exp(-10650/T)<br>k(inf) = 4.80E+15 exp(-11170/T) | 8.31E-2 |
| 50 | PNA = 0.59 HO2 + 0.59 NO2 + 0.41 OH + 0.41 NO3 | Photolysis | 2.36E-6 |
| 51 | PNA + OH = NO2 | k = 3.20E-13 exp(690/T) | 3.24E-12 |
| 52 | SO2 + OH = SULF + HO2 | Falloff: F=0.53; n=1.1<br>k(0) = 4.50E-31 (T/300)^-3.9<br>k(inf) = 1.30E-12 (T/300)^-0.7 | 8.12E-13 |
| 53 | C2O3 + NO = NO2 + MEO2 + RO2 | k = 7.50E-12 exp(290/T) | 1.98E-11 |
| 54 | C2O3 + NO2 = PAN | Falloff: F=0.3; n=1.41<br>k(0) = 2.70E-28 (T/300)^-7.1<br>k(inf) = 1.20E-11 (T/300)^-0.9 | 9.40E-12 |
| 55 | PAN = NO2 + C2O3 | Falloff: F=0.3; n=1.41<br>k(0) = 4.90E-3 exp(-12100/T)<br>k(inf) = 5.40E+16 exp(-13830/T) | 2.98E-4 |
| 56 | PAN = 0.6 NO2 + 0.6 C2O3 + 0.4 NO3 + 0.4 MEO2 + 0.4 RO2 | Photolysis | 3.47E-7 |
| 57 | C2O3 + HO2 = 0.41 PACD + 0.15 AACD + 0.15 O3 + 0.44 MEO2 + 0.44 RO2 + 0.44 OH | k = 5.20E-13 exp(980/T) | 1.39E-11 |
| 58 | C2O3 + RO2 = C2O3 | k = 8.90E-13 exp(800/T) | 1.30E-11 |
| 59 | C2O3 + C2O3 = 2 MEO2 + 2 RO2 | k = 2.90E-12 exp(500/T) | 1.55E-11 |
| 60 | C2O3 + CXO3 = MEO2 + ALD2 + XO2H + 2 RO2 | k = 2.90E-12 exp(500/T) | 1.55E-11 |

| Number | Reactants and Products | Rate Constant Expression | $k_{298}$ |
|---|---|---|---|
| 61 | CXO3 + NO = NO2 + ALD2 + XO2H + RO2 | k = 6.70E-12 exp(340/T) | 2.10E-11 |
| 62 | CXO3 + NO2 = PANX | k = k(ref) K<br>k(ref) = k(54)<br>K = 1.00E+0 | 9.40E-12 |
| 63 | PANX = NO2 + CXO3 | k = k(ref) K<br>k(ref) = k(55)<br>K = 1.00E+0 | 2.98E-4 |
| 64 | PANX = 0.6 NO2 + 0.6 CXO3 + 0.4 NO3 + 0.4 ALD2 + 0.4 XO2H + 0.4 RO2 | Photolysis | 3.47E-7 |
| 65 | CXO3 + HO2 = 0.41 PACD + 0.15 AACD + 0.15 O3 + 0.44 ALD2 + 0.44 XO2H + 0.44 RO2 + 0.44 OH | k = 5.20E-13 exp(980/T) | 1.39E-11 |
| 66 | CXO3 + RO2 = 0.8 ALD2 + 0.8 XO2H + 0.8 RO2 | k = 8.90E-13 exp(800/T) | 1.30E-11 |
| 67 | CXO3 + CXO3 = 2 ALD2 + 2 XO2H + 2 RO2 | k = 3.20E-12 exp(500/T) | 1.71E-11 |
| 68 | RO2 + NO = NO | k = 2.40E-12 exp(360/T) | 8.03E-12 |
| 69 | RO2 + HO2 = HO2 | k = 4.80E-13 exp(800/T) | 7.03E-12 |
| 70 | RO2 + RO2 = | k = 6.50E-14 exp(500/T) | 3.48E-13 |
| 71 | MEO2 + NO = FORM + HO2 + NO2 | k = 2.30E-12 exp(360/T) | 7.70E-12 |
| 72 | MEO2 + HO2 = 0.9 MEPX + 0.1 FORM | k = 3.80E-13 exp(780/T) | 5.21E-12 |
| 73 | MEO2 + C2O3 = FORM + 0.9 HO2 + 0.9 MEO2 + 0.1 AACD + 0.9 RO2 | k = 2.00E-12 exp(500/T) | 1.07E-11 |
| 74 | MEO2 + RO2 = 0.685 FORM + 0.315 MEOH + 0.37 HO2 + RO2 | k = k(ref) K<br>k(ref) = k(70)<br>K = 1.00E+0 | 3.48E-13 |
| 75 | XO2H + NO = NO2 + HO2 | k = 2.70E-12 exp(360/T) | 9.04E-12 |
| 76 | XO2H + HO2 = ROOH | k = 6.80E-13 exp(800/T) | 9.96E-12 |
| 77 | XO2H + C2O3 = 0.8 HO2 + 0.8 MEO2 + 0.2 AACD + 0.8 RO2 | k = k(ref) K<br>k(ref) = k(58)<br>K = 1.00E+0 | 1.30E-11 |
| 78 | XO2H + RO2 = 0.6 HO2 + RO2 | k = k(ref) K<br>k(ref) = k(70)<br>K = 1.00E+0 | 3.48E-13 |
| 79 | XO2 + NO = NO2 | k = k(ref) K<br>k(ref) = k(75)<br>K = 1.00E+0 | 9.04E-12 |
| 80 | XO2 + HO2 = ROOH | k = k(ref) K<br>k(ref) = k(76)<br>K = 1.00E+0 | 9.96E-12 |
| 81 | XO2 + C2O3 = 0.8 MEO2 + 0.2 AACD + 0.8 RO2 | k = k(ref) K<br>k(ref) = k(58)<br>K = 1.00E+0 | 1.30E-11 |
| 82 | XO2 + RO2 = RO2 | k = k(ref) K<br>k(ref) = k(70)<br>K = 1.00E+0 | 3.48E-13 |
| 83 | XO2N + NO = 0.5 NTR1 + 0.5 NTR2 | k = k(ref) K<br>k(ref) = k(75)<br>K = 1.00E+0 | 9.04E-12 |
| 84 | XO2N + HO2 = ROOH | k = k(ref) K<br>k(ref) = k(76)<br>K = 1.00E+0 | 9.96E-12 |

| Number | Reactants and Products | Rate Constant Expression | $k_{298}$ |
|---|---|---|---|
| 85 | XO2N + C2O3 = 0.8 HO2 + 0.8 MEO2 + 0.2 AACD + 0.8 RO2 | k = k(ref) K<br>k(ref) = k(58)<br>K = 1.00E+0 | 1.30E-11 |
| 86 | XO2N + RO2 = RO2 | k = k(ref) K<br>k(ref) = k(70)<br>K = 1.00E+0 | 3.48E-13 |
| 87 | MEPX + OH = 0.6 MEO2 + 0.6 RO2 + 0.4 FORM + 0.4 OH | k = 5.30E-12 exp(190/T) | 1.00E-11 |
| 88 | MEPX = MEO2 + RO2 + OH | Photolysis | 2.68E-6 |
| 89 | ROOH + OH = 0.54 XO2H + 0.06 XO2N + 0.6 RO2 + 0.4 OH | k = 5.30E-12 exp(190/T) | 1.00E-11 |
| 90 | ROOH = HO2 + OH | Photolysis | 2.68E-6 |
| 91 | NTR1 + OH = NTR2 | k = 2.00E-12 | 2.00E-12 |
| 92 | NTR1 = NO2 | Photolysis | 1.06E-6 |
| 93 | FACD + OH = HO2 | k = 4.50E-13 | 4.50E-13 |
| 94 | AACD + OH = MEO2 + RO2 | k = 4.00E-14 exp(850/T) | 6.93E-13 |
| 95 | PACD + OH = C2O3 | k = 5.30E-12 exp(190/T) | 1.00E-11 |
| 96 | FORM + OH = HO2 + CO | k = 5.40E-12 exp(135/T) | 8.49E-12 |
| 97 | FORM = 2 HO2 + CO | Photolysis | 1.78E-5 |
| 98 | FORM = CO + H2 | Photolysis | 2.38E-5 |
| 99 | FORM + NO3 = HNO3 + HO2 + CO | k = 5.50E-16 | 5.50E-16 |
| 100 | FORM + HO2 = HCO3 | k = 9.70E-15 exp(625/T) | 7.90E-14 |
| 101 | HCO3 = FORM + HO2 | k = 2.40E+12 exp(-7000/T) | 1.51E+2 |
| 102 | HCO3 + NO = FACD + NO2 + HO2 | k = 5.60E-12 | 5.60E-12 |
| 103 | HCO3 + HO2 = 0.5 MEPX + 0.5 FACD + 0.2 OH + 0.2 HO2 | k = 5.60E-15 exp(2300/T) | 1.26E-11 |
| 104 | ALD2 + OH = C2O3 | k = 4.70E-12 exp(345/T) | 1.50E-11 |
| 105 | ALD2 + NO3 = C2O3 + HNO3 | k = 1.40E-12 exp(-1860/T) | 2.73E-15 |
| 106 | ALD2 = MEO2 + RO2 + CO + HO2 | Photolysis | 1.76E-6 |
| 107 | ALDX + OH = CXO3 | k = 4.90E-12 exp(405/T) | 1.91E-11 |
| 108 | ALDX + NO3 = CXO3 + HNO3 | k = 6.30E-15 | 6.30E-15 |
| 109 | ALDX = ALD2 + XO2H + RO2 + CO + HO2 | Photolysis | 6.96E-6 |
| 110 | GLYD + OH = 0.2 GLY + 0.2 HO2 + 0.8 C2O3 | k = 8.00E-12 | 8.00E-12 |
| 111 | GLYD = 0.74 FORM + 0.89 CO + 1.4 HO2 + 0.15 MEOH + 0.19 OH + 0.11 GLY + 0.11 XO2H + 0.11 RO2 | Photolysis | 1.56E-6 |
| 112 | GLYD + NO3 = HNO3 + C2O3 | k = 1.40E-12 exp(-1860/T) | 2.73E-15 |
| 113 | GLY + OH = 1.8 CO + 0.2 XO2 + 0.2 RO2 + HO2 | k = 3.10E-12 exp(340/T) | 9.70E-12 |
| 114 | GLY = 2 HO2 + 2 CO | Photolysis | 5.50E-5 |
| 115 | GLY + NO3 = HNO3 + 1.5 CO + 0.5 XO2 + 0.5 RO2 + HO2 | k = 1.40E-12 exp(-1860/T) | 2.73E-15 |
| 116 | MGLY = C2O3 + HO2 + CO | Photolysis | 1.46E-4 |
| 117 | MGLY + NO3 = HNO3 + C2O3 + XO2 + RO2 | k = 1.40E-12 exp(-1860/T) | 2.73E-15 |
| 118 | MGLY + OH = C2O3 + CO | k = 1.90E-12 exp(575/T) | 1.31E-11 |
| 119 | H2 + OH = HO2 | k = 7.70E-12 exp(-2100/T) | 6.70E-15 |
| 120 | CO + OH = HO2 | k = k1 + k2 [M]<br>k1 = 1.44E-13<br>k2 = 3.43E-33 | 2.28E-13 |
| 121 | CH4 + OH = MEO2 + RO2 | k = 1.85E-12 exp(-1690/T) | 6.37E-15 |

| Number | Reactants and Products | Rate Constant Expression | $k_{298}$ |
|---|---|---|---|
| 122 | ETHA + OH = 0.991 ALD2 + 0.991 XO2H + 0.009 XO2N + RO2 | k = 6.90E-12 exp(-1000/T) | 2.41E-13 |
| 123 | MEOH + OH = FORM + HO2 | k = 2.85E-12 exp(-345/T) | 8.95E-13 |
| 124 | ETOH + OH = 0.95 ALD2 + 0.9 HO2 + 0.1 XO2H + 0.1 RO2 + 0.078 FORM + 0.011 GLYD | k = 3.00E-12 exp(20/T) | 3.21E-12 |
| 125 | KET = 0.5 ALD2 + 0.5 C2O3 + 0.5 XO2H + 0.5 CXO3 + 0.5 MEO2 + RO2 - 2.5 PAR | Photolysis | 2.27E-7 |
| 126 | ACET = 0.38 CO + 1.38 MEO2 + 1.38 RO2 + 0.62 C2O3 | Photolysis | 2.08E-7 |
| 127 | ACET + OH = FORM + C2O3 + XO2 + RO2 | k = 1.41E-12 exp(-620.6/T) | 1.76E-13 |
| 128 | PRPA + OH = XPRP | k = 7.60E-12 exp(-585/T) | 1.07E-12 |
| 129 | PAR + OH = XPAR | k = 8.10E-13 | 8.10E-13 |
| 130 | ROR = 0.2 KET + 0.42 ACET + 0.74 ALD2 + 0.37 ALDX + 0.04 XO2N + 0.94 XO2H + 0.98 RO2 + 0.02 ROR - 2.7 PAR | k = 5.70E+12 exp(-5780/T) | 2.15E+4 |
| 131 | ROR + O2 = KET + HO2 | k = 1.50E-14 exp(-200/T) | 7.67E-15 |
| 132 | ROR + NO2 = NTR1 | k = 8.60E-12 exp(400/T) | 3.29E-11 |
| 133 | ETHY + OH = 0.7 GLY + 0.7 OH + 0.3 FACD + 0.3 CO + 0.3 HO2 | Falloff: F=0.37; n=1.3<br>k(0) = 5.00E-30 (T/300)^-1.5<br>k(inf) = 1.00E-12 | 7.52E-13 |
| 134 | ETH + OH = XO2H + RO2 + 1.56 FORM + 0.22 GLYD | Falloff: F=0.48; n=1.15<br>k(0) = 8.60E-29 (T/300)^-3.1<br>k(inf) = 9.00E-12 (T/300)^-0.85 | 7.84E-12 |
| 135 | ETH + O3 = FORM + 0.51 CO + 0.16 HO2 + 0.16 OH + 0.37 FACD | k = 9.10E-15 exp(-2580/T) | 1.58E-18 |
| 136 | ETH + NO3 = 0.5 NO2 + 0.5 NTR1 + 0.5 XO2H + 0.5 XO2 + RO2 + 1.125 FORM | k = 3.30E-12 exp(-2880/T) | 2.10E-16 |
| 137 | OLE + OH = 0.781 FORM + 0.488 ALD2 + 0.488 ALDX + 0.976 XO2H + 0.195 XO2 + 0.024 XO2N + 1.195 RO2 - 0.73 PAR | Falloff: F=0.5; n=1.13<br>k(0) = 8.00E-27 (T/300)^-3.5<br>k(inf) = 3.00E-11 (T/300)^-1 | 2.86E-11 |
| 138 | OLE + O3 = 0.295 ALD2 + 0.555 FORM + 0.27 ALDX + 0.15 XO2H + 0.15 RO2 + 0.334 OH + 0.08 HO2 + 0.378 CO + 0.075 GLY + 0.075 MGLY + 0.09 FACD + 0.13 AACD + 0.04 H2O2 - 0.79 PAR | k = 5.50E-15 exp(-1880/T) | 1.00E-17 |
| 139 | OLE + NO3 = 0.5 NO2 + 0.5 NTR1 + 0.48 XO2 + 0.48 XO2H + 0.04 XO2N + RO2 + 0.5 FORM + 0.25 ALD2 + 0.375 ALDX - 1 PAR | k = 4.60E-13 exp(-1155/T) | 9.54E-15 |
| 140 | IOLE + OH = 1.3 ALD2 + 0.7 ALDX + XO2H + RO2 | k = 1.05E-11 exp(519/T) | 5.99E-11 |
| 141 | IOLE + O3 = 0.732 ALD2 + 0.442 ALDX + 0.128 FORM + 0.245 CO + 0.5 OH + 0.3 XO2H + 0.3 RO2 + 0.24 GLY + 0.06 MGLY + 0.29 PAR + 0.08 AACD + 0.08 H2O2 | k = 4.70E-15 exp(-1013/T) | 1.57E-16 |
| 142 | IOLE + NO3 = 0.5 NO2 + 0.5 NTR1 + 0.48 XO2 + 0.48 XO2H + 0.04 XO2N + RO2 + 0.5 ALD2 + 0.625 ALDX + PAR | k = 3.70E-13 | 3.70E-13 |
| 143 | ISOP + OH = ISO2 + RO2 | k = 2.70E-11 exp(390/T) | 9.99E-11 |

| Number | Reactants and Products | Rate Constant Expression | $k_{298}$ |
|---|---|---|---|
| 144 | ISO2 + NO = 0.1 INTR + 0.9 NO2 + 0.673 FORM + 0.9 ISPD + 0.818 HO2 + 0.082 XO2H + 0.082 RO2 | k = 2.39E-12 exp(365/T) | 8.13E-12 |
| 145 | ISO2 + HO2 = 0.88 ISPX + 0.12 OH + 0.12 HO2 + 0.12 FORM + 0.12 ISPD | k = 7.43E-13 exp(700/T) | 7.78E-12 |
| 146 | ISO2 + C2O3 = 0.598 FORM + 1 ISPD + 0.728 HO2 + 0.072 XO2H + 0.8 MEO2 + 0.2 AACD + 0.872 RO2 | k = k(ref) K<br>k(ref) = k(58)<br>K = 1.00E+0 | 1.30E-11 |
| 147 | ISO2 + RO2 = 0.598 FORM + 1 ISPD + 0.728 HO2 + 0.072 XO2H + 1.072 RO2 | k = k(ref) K<br>k(ref) = k(70)<br>K = 1.00E+0 | 3.48E-13 |
| 148 | ISO2 = HO2 + HPLD | k = 3.30E+9 exp(-8300/T) | 2.64E-3 |
| 149 | ISOP + O3 = 0.6 FORM + 0.65 ISPD + 0.15 ALDX + 0.2 CXO3 + 0.35 PAR + 0.266 OH + 0.2 XO2 + 0.2 RO2 + 0.066 HO2 + 0.066 CO | k = 1.03E-14 exp(-1995/T) | 1.27E-17 |
| 150 | ISOP + NO3 = 0.35 NO2 + 0.65 NTR2 + 0.64 XO2H + 0.33 XO2 + 0.03 XO2N + RO2 + 0.35 FORM + 0.35 ISPD | k = 3.03E-12 exp(-448/T) | 6.74E-13 |
| 151 | ISPD + OH = 0.022 XO2N + 0.521 XO2 + 0.115 MGLY + 0.115 MEO2 + 0.269 GLYD + 0.269 C2O3 + 0.457 OPO3 + 0.117 PAR + 0.137 ACET + 0.137 CO + 0.137 HO2 + 0.658 RO2 | k = 5.58E-12 exp(511/T) | 3.10E-11 |
| 152 | ISPD + O3 = 0.04 ALD2 + 0.231 FORM + 0.531 MGLY + 0.17 GLY + 0.17 ACET + 0.543 CO + 0.461 OH + 0.15 FACD + 0.398 HO2 + 0.143 C2O3 | k = 3.88E-15 exp(-1770/T) | 1.02E-17 |
| 153 | ISPD + NO3 = 0.717 HNO3 + 0.142 NTR2 + 0.142 NO2 + 0.142 XO2 + 0.142 XO2H + 0.113 GLYD + 0.113 MGLY + 0.717 PAR + 0.717 CXO3 + 0.284 RO2 | k = 4.10E-12 exp(-1860/T) | 7.98E-15 |
| 154 | ISPD = 0.76 HO2 + 0.34 XO2H + 0.16 XO2 + 0.34 MEO2 + 0.208 C2O3 + 0.26 FORM + 0.24 OLE + 0.24 PAR + 0.17 ACET + 0.128 GLYD + 0.84 RO2 | Photolysis | 1.60E-5 |
| 155 | ISPX + OH = 0.904 EPOX + 0.933 OH + 0.067 ISO2 + 0.067 RO2 + 0.029 IOLE + 0.029 ALDX | k = 2.23E-11 exp(372/T) | 7.77E-11 |
| 156 | HPLD = OH + ISPD | Photolysis | 4.41E-4 |
| 157 | HPLD + NO3 = HNO3 + ISPD | k = 6.00E-12 exp(-1860/T) | 1.17E-14 |
| 158 | EPOX + OH = EPX2 + RO2 | k = 5.78E-11 exp(-400/T) | 1.51E-11 |
| 159 | EPX2 + HO2 = 0.275 GLYD + 0.275 GLY + 0.275 MGLY + 1.125 OH + 0.825 HO2 + 0.375 FORM + 0.074 FACD + 0.251 CO + 2.175 PAR | k = 7.43E-13 exp(700/T) | 7.78E-12 |
| 160 | EPX2 + NO = 0.275 GLYD + 0.275 GLY + 0.275 MGLY + 0.125 OH + 0.825 HO2 + 0.375 FORM + NO2 + 0.251 CO + 2.175 PAR | k = 2.39E-12 exp(365/T) | 8.13E-12 |

| Number | Reactants and Products | Rate Constant Expression | $k_{298}$ |
|---|---|---|---|
| 161 | EPX2 + C2O3 = 0.22 GLYD + 0.22 GLY + 0.22 MGLY + 0.1 OH + 0.66 HO2 + 0.3 FORM + 0.2 CO + 1.74 PAR + 0.8 MEO2 + 0.2 AACD + 0.8 RO2 | k = k(ref) K<br>k(ref) = k(58)<br>K = 1.00E+0 | 1.30E-11 |
| 162 | EPX2 + RO2 = 0.275 GLYD + 0.275 GLY + 0.275 MGLY + 0.125 OH + 0.825 HO2 + 0.375 FORM + 0.251 CO + 2.175 PAR + RO2 | k = k(ref) K<br>k(ref) = k(70)<br>K = 1.00E+0 | 3.48E-13 |
| 163 | INTR + OH = 0.63 XO2 + 0.37 XO2H + RO2 + 0.444 NO2 + 0.185 NO3 + 0.104 INTR + 0.592 FORM + 0.331 GLYD + 0.185 FACD + 2.7 PAR + 0.098 OLE + 0.078 ALDX + 0.266 NTR2 | k = 3.10E-11 | 3.10E-11 |
| 164 | TERP + OH = 0.75 XO2H + 0.5 XO2 + 0.25 XO2N + 1.5 RO2 + 0.28 FORM + 1.66 PAR + 0.47 ALDX | k = 1.50E-11 exp(449/T) | 6.77E-11 |
| 165 | TERP + O3 = 0.57 OH + 0.07 XO2H + 0.69 XO2 + 0.18 XO2N + 0.94 RO2 + 0.24 FORM + 0.001 CO + 7 PAR + 0.21 ALDX + 0.39 CXO3 | k = 1.20E-15 exp(-821/T) | 7.63E-17 |
| 166 | TERP + NO3 = 0.47 NO2 + 0.28 XO2H + 0.75 XO2 + 0.25 XO2N + 1.28 RO2 + 0.47 ALDX + 0.53 NTR2 | k = 3.70E-12 exp(175/T) | 6.66E-12 |
| 167 | BENZ + OH = 0.53 CRES + 0.352 BZO2 + 0.352 RO2 + 0.118 OPEN + 0.118 OH + 0.53 HO2 | k = 2.30E-12 exp(-190/T) | 1.22E-12 |
| 168 | BZO2 + NO = 0.918 NO2 + 0.082 NTR2 + 0.918 GLY + 0.918 OPEN + 0.918 HO2 | k = 2.70E-12 exp(360/T) | 9.04E-12 |
| 169 | BZO2 + C2O3 = GLY + OPEN + HO2 + MEO2 + RO2 | k = k(ref) K<br>k(ref) = k(58)<br>K = 1.00E+0 | 1.30E-11 |
| 170 | BZO2 + HO2 = | k = 1.90E-13 exp(1300/T) | 1.49E-11 |
| 171 | BZO2 + RO2 = GLY + OPEN + HO2 + RO2 | k = k(ref) K<br>k(ref) = k(70)<br>K = 1.00E+0 | 3.48E-13 |
| 172 | TOL + OH = 0.18 CRES + 0.65 TO2 + 0.72 RO2 + 0.1 OPEN + 0.1 OH + 0.07 XO2H + 0.18 HO2 | k = 1.80E-12 exp(340/T) | 5.63E-12 |
| 173 | TO2 + NO = 0.86 NO2 + 0.14 NTR2 + 0.417 GLY + 0.443 MGLY + 0.66 OPEN + 0.2 XOPN + 0.86 HO2 | k = 2.70E-12 exp(360/T) | 9.04E-12 |
| 174 | TO2 + C2O3 = 0.48 GLY + 0.52 MGLY + 0.77 OPEN + 0.23 XOPN + HO2 + MEO2 + RO2 | k = k(ref) K<br>k(ref) = k(58)<br>K = 1.00E+0 | 1.30E-11 |
| 175 | TO2 + HO2 = | k = 1.90E-13 exp(1300/T) | 1.49E-11 |
| 176 | TO2 + RO2 = 0.48 GLY + 0.52 MGLY + 0.77 OPEN + 0.23 XOPN + HO2 + RO2 | k = k(ref) K<br>k(ref) = k(70)<br>K = 1.00E+0 | 3.48E-13 |
| 177 | XYL + OH = 0.155 CRES + 0.544 XLO2 + 0.602 RO2 + 0.244 XOPN + 0.244 OH + 0.058 XO2H + 0.155 HO2 | k = 1.85E-11 | 1.85E-11 |

| Number | Reactants and Products | Rate Constant Expression | $k_{298}$ |
|---|---|---|---|
| 178 | XLO2 + NO = 0.86 NO2 + 0.14 NTR2 + 0.221 GLY + 0.675 MGLY + 0.3 OPEN + 0.56 XOPN + 0.86 HO2 | k = 2.70E-12 exp(360/T) | 9.04E-12 |
| 179 | XLO2 + HO2 = | k = 1.90E-13 exp(1300/T) | 1.49E-11 |
| 180 | XLO2 + C2O3 = 0.26 GLY + 0.77 MGLY + 0.35 OPEN + 0.65 XOPN + HO2 + MEO2 + RO2 | k = k(ref) K<br>k(ref) = k(58)<br>K = 1.00E+0 | 1.30E-11 |
| 181 | XLO2 + RO2 = 0.26 GLY + 0.77 MGLY + 0.35 OPEN + 0.65 XOPN + HO2 + RO2 | k = k(ref) K<br>k(ref) = k(70)<br>K = 1.00E+0 | 3.48E-13 |
| 182 | CRES + OH = 0.025 GLY + 0.025 OPEN + HO2 + 0.2 CRO + 0.732 CAT1 + 0.02 XO2N + 0.02 RO2 | k = 1.70E-12 exp(950/T) | 4.12E-11 |
| 183 | CRES + NO3 = 0.3 CRO + HNO3 + 0.48 XO2 + 0.12 XO2H + 0.24 GLY + 0.24 MGLY + 0.48 OPO3 + 0.1 XO2N + 0.7 RO2 | k = 1.40E-11 | 1.40E-11 |
| 184 | CRO + NO2 = CRON | k = 2.10E-12 | 2.10E-12 |
| 185 | CRO + HO2 = CRES | k = 5.50E-12 | 5.50E-12 |
| 186 | CRON + OH = NTR2 + 0.5 CRO | k = 1.53E-12 | 1.53E-12 |
| 187 | CRON + NO3 = NTR2 + 0.5 CRO + HNO3 | k = 3.80E-12 | 3.80E-12 |
| 188 | CRON = HONO + HO2 + FORM + OPEN | Photolysis | 9.45E-5 |
| 189 | XOPN = 0.4 GLY + XO2H + 0.7 HO2 + 0.7 CO + 0.3 C2O3 | Photolysis | 5.04E-4 |
| 190 | XOPN + OH = MGLY + 0.4 GLY + 2 XO2H + 2 RO2 | k = 9.00E-11 | 9.00E-11 |
| 191 | XOPN + O3 = 1.2 MGLY + 0.5 OH + 0.6 C2O3 + 0.1 ALD2 + 0.5 CO + 0.3 XO2H + 0.3 RO2 | k = 1.08E-16 exp(-500/T) | 2.02E-17 |
| 192 | XOPN + NO3 = 0.5 NO2 + 0.5 NTR2 + 0.45 XO2H + 0.45 XO2 + 0.1 XO2N + RO2 + 0.25 OPEN + 0.25 MGLY | k = 3.00E-12 | 3.00E-12 |
| 193 | OPEN = OPO3 + HO2 + CO | Photolysis | 5.04E-4 |
| 194 | OPEN + OH = 0.6 OPO3 + 0.4 XO2H + 0.4 RO2 + 0.4 GLY | k = 4.40E-11 | 4.40E-11 |
| 195 | OPEN + O3 = 1.4 GLY + 0.24 MGLY + 0.5 OH + 0.12 C2O3 + 0.08 FORM + 0.02 ALD2 + 1.98 CO + 0.56 HO2 | k = 5.40E-17 exp(-500/T) | 1.01E-17 |
| 196 | OPEN + NO3 = OPO3 + HNO3 | k = 3.80E-12 | 3.80E-12 |
| 197 | CAT1 + OH = 0.14 FORM + 0.2 HO2 + 0.5 CRO | k = 5.00E-11 | 5.00E-11 |
| 198 | CAT1 + NO3 = CRO + HNO3 | k = 1.70E-10 | 1.70E-10 |
| 199 | OPO3 + NO = NO2 + 0.5 GLY + 0.5 CO + 0.8 HO2 + 0.2 CXO3 | k = 1.00E-11 | 1.00E-11 |
| 200 | OPO3 + NO2 = OPAN | k = k(ref) K<br>k(ref) = k(54)<br>K = 1.00E+0 | 9.40E-12 |
| 201 | OPAN = OPO3 + NO2 | k = k(ref) K<br>k(ref) = k(55)<br>K = 1.00E+0 | 2.98E-4 |
| 202 | OPO3 + HO2 = 0.41 PACD + 0.15 AACD + 0.15 O3 + 0.44 ALDX + 0.44 XO2H + 0.44 RO2 + 0.44 OH | k = k(ref) K<br>k(ref) = k(57)<br>K = 1.00E+0 | 1.39E-11 |

| Number | Reactants and Products | Rate Constant Expression | $k_{298}$ |
|---|---|---|---|
| 203 | OPO3 + C2O3 = MEO2 + XO2 + ALDX + 2 RO2 | k = k(ref) K<br>k(ref) = k(59)<br>K = 1.00E+0 | 1.55E-11 |
| 204 | OPO3 + RO2 = 0.8 XO2H + 0.8 ALDX + 1.8 RO2 + 0.2 AACD | k = k(ref) K<br>k(ref) = k(58)<br>K = 1.00E+0 | 1.30E-11 |
| 205 | OPAN + OH = 0.5 NO2 + 0.5 GLY + CO + 0.5 NTR2 | k = 3.60E-11 | 3.60E-11 |
| 206 | PANX + OH = ALD2 + NO2 | k = 3.00E-12 | 3.00E-12 |
| 207 | NTR2 = HNO3 | k = 2.30E-5 | 2.30E-5 |
| 208 | ECH4 + OH = MEO2 + RO2 | k = 1.85E-12 exp(-1690/T) | 6.37E-15 |
| 209 | I2 = 2 I | Photolysis | 1.44E-1 |
| 210 | HOI = I + OH | Photolysis | 6.36E-2 |
| 211 | I + O3 = IO | k = 2.10E-11 exp(-830/T) | 1.30E-12 |
| 212 | IO = I + O | Photolysis | 1.18E-1 |
| 213 | IO + IO = 0.4 I + 0.4 OIO + 0.6 I2O2 | k = 5.40E-11 exp(180/T) | 9.88E-11 |
| 214 | IO + HO2 = HOI | k = 1.40E-11 exp(540/T) | 8.57E-11 |
| 215 | IO + NO = I + NO2 | k = 7.15E-12 exp(300/T) | 1.96E-11 |
| 216 | IO + NO2 = INO3 | Falloff: F=0.4; n=1<br>k(0) = 7.70E-31 (T/300)^-5<br>k(inf) = 1.60E-11 | 3.55E-12 |
| 217 | OIO = I | Photolysis | 1.41E-1 |
| 218 | OIO + OH = HIO3 | Falloff: F=0.3; n=1<br>k(0) = 1.50E-27 (T/300)^-3.93<br>k(inf) = 5.50E-10 exp(46/T) | 4.72E-10 |
| 219 | OIO + IO = IXOY | k = 1.00E-10 | 1.00E-10 |
| 220 | OIO + NO = IO + NO2 | k = 1.10E-12 exp(542/T) | 6.78E-12 |
| 221 | I2O2 = I + OIO | k = 1.00E+1 | 1.00E+1 |
| 222 | I2O2 + O3 = IXOY | k = 1.00E-12 | 1.00E-12 |
| 223 | INO3 = I + NO3 | Photolysis | 1.25E-2 |
| 224 | INO3 + H2O = HOI + HNO3 | k = 2.50E-22 | 2.50E-22 |
| 225 | XPRP = XO2N + RO2 | Falloff: F=0.41; n=1<br>k(0) = 2.37E-21<br>k(inf) = 4.30E-1 (T/298)^-8 | 3.09E-2 |
| 226 | XPRP = 0.732 ACET + 0.268 ALDX + 0.268 PAR + XO2H + RO2 | k = 1.00E+0 | 1.00E+0 |
| 227 | XPAR = XO2N + RO2 | Falloff: F=0.41; n=1<br>k(0) = 4.81E-20<br>k(inf) = 4.30E-1 (T/298)^-8 | 1.49E-1 |
| 228 | XPAR = 0.126 ALDX + 0.874 ROR + 0.126 XO2H + 0.874 XO2 + RO2 - 0.126 PAR | k = 1.00E+0 | 1.00E+0 |
| 229 | INTR = HNO3 | k = 1.40E-4 | 1.40E-4 |

**Table A-2. CB6r4 species names and descriptions**

| Species | Description | Carbon # | C | H | O | N | I | MW |
|---|---|---|---|---|---|---|---|---|
| BZO2 | Peroxy radical from OH addition to benzene | 6 | 6 | 7 | 5 | | | 159.06 |
| C2O3 | Acetylperoxy radical | 2 | 2 | 3 | 3 | | | 75.01 |
| CRO | Alkoxy radical from cresol | 7 | 7 | 7 | 1 | | | 107.11 |
| CXO3 | C3 and higher acylperoxy radicals | 3 | 3 | 5 | 3 | | | 89.04 |
| EPX2 | Peroxy radical from EPOX reaction with OH | 5 | 5 | 9 | 5 | | | 149.06 |
| HCO3 | Adduct from HO2 plus formaldehyde | 1 | 1 | 3 | 3 | | | 63.00 |
| HO2 | Hydroperoxy radical | | | 1 | 2 | | | 32.99 |
| ISO2 | Peroxy radical from OH addition to isoprene | 5 | 5 | 9 | 3 | | | 117.08 |
| MEO2 | Methylperoxy radical | 1 | 1 | 3 | 2 | | | 47.01 |
| O | Oxygen atom in the O3(P) electronic state | | | | 1 | | | 15.99 |
| O1D | Oxygen atom in the O1(D) electronic state | | | | 1 | | | 15.99 |
| OH | Hydroxyl radical | | | 1 | 1 | | | 17.00 |
| OPO3 | Peroxyacyl radical from OPEN | 4 | 4 | 3 | 4 | | | 115.02 |
| RO2 | Operator to approximate total peroxy radical concentration | | 4 | 7 | 2 | | | 87.07 |
| ROR | Secondary alkoxy radical | 1 | 4 | 7 | 1 | | | 71.08 |
| TO2 | Peroxy radical from OH addition to TOL | 7 | 7 | 9 | 5 | | | 173.08 |
| XLO2 | Peroxy radical from OH addition to XYL | 8 | 8 | 11 | 5 | | | 187.11 |
| XO2 | NO to NO2 conversion from alkylperoxy (RO2) radical | | 4 | 7 | 2 | | | 87.07 |
| XO2H | NO to NO2 conversion (XO2) accompanied by HO2 production | | 4 | 7 | 2 | | | 87.07 |
| XO2N | NO to organic nitrate conversion from alkylperoxy (RO2) radical | | 4 | 7 | 2 | | | 87.07 |
| I | Iodine atom | | | | | | 1 | 126.90 |
| IO | Iodine monoxide | | | | 1 | | 1 | 142.89 |
| OIO | Iodine dioxide | | | | 2 | | 1 | 158.88 |
| XPRP | Operator for organic nitrates from PRPA | 3 | 3 | 7 | 2 | 1 | | 89.06 |
| XPAR | Operator for organic nitrates from PAR | 1 | 5 | 11 | 2 | 1 | | 117.11 |
| AACD | Acetic acid | 2 | 2 | 4 | 2 | | | 60.03 |
| ACET | Acetone | 3 | 3 | 6 | 1 | | | 58.06 |
| ALD2 | Acetaldehyde | 2 | 2 | 4 | 1 | | | 44.04 |
| ALDX | Propionaldehyde and higher aldehydes | 3 | 3 | 6 | 1 | | | 58.06 |
| BENZ | Benzene | 6 | 6 | 6 | | | | 78.10 |
| CAT1 | Methyl-catechols | 7 | 7 | 8 | 2 | | | 124.11 |
| CO | Carbon monoxide | 1 | 1 | | 1 | | | 28.00 |
| CRES | Cresols | 7 | 7 | 8 | 1 | | | 108.12 |
| CRON | Nitro-cresols | 7 | 7 | 7 | 3 | 1 | | 153.09 |
| EPOX | Epoxide formed from ISPX reaction with OH | 5 | 5 | 10 | 3 | | | 118.09 |
| ETH | Ethene | 2 | 2 | 4 | | | | 28.05 |
| ETHA | Ethane | 2 | 2 | 6 | | | | 30.06 |
| ETHY | Ethyne | 2 | 2 | 2 | | | | 26.03 |
| ETOH | Ethanol | 2 | 2 | 6 | 1 | | | 46.05 |
| FACD | Formic acid | 1 | 1 | 2 | 2 | | | 46.00 |
| FORM | Formaldehyde | 1 | 1 | 2 | 1 | | | 30.01 |
| GLY | Glyoxal | 2 | 2 | 2 | 2 | | | 58.01 |
| GLYD | Glycolaldehyde | 2 | 2 | 4 | 2 | | | 60.03 |
| H2O2 | Hydrogen peroxide | | | 2 | 2 | | | 33.99 |
| HNO3 | Nitric acid | | | 1 | 3 | 1 | | 62.98 |

| Species | Description | Carbon # | C | H | O | N | I | MW |
|---|---|---|---|---|---|---|---|---|
| HONO | Nitrous acid | | | 1 | 2 | 1 | | 46.99 |
| HPLD | hydroperoxyaldehyde | 5 | 5 | 8 | 3 | | | 116.08 |
| INTR | Organic nitrates from ISO2 reaction with NO | 5 | 5 | 9 | 4 | 1 | | 147.07 |
| IOLE | Internal olefin carbon bond (R-C=C-R) | 4 | 4 | 8 | | | | 56.10 |
| ISOP | Isoprene | 5 | 5 | 8 | | | | 68.11 |
| ISPD | Isoprene product (lumped methacrolein, methyl vinyl ketone, etc.) | 4 | 4 | 6 | 1 | | | 70.07 |
| ISPX | Hydroperoxides from ISO2 reaction with HO2 | 5 | 5 | 10 | 3 | | | 118.09 |
| KET | Ketone carbon bond (C=O) | 4 | 4 | 8 | 1 | | | 72.09 |
| MEOH | Methanol | 1 | 1 | 4 | 1 | | | 32.03 |
| MEPX | Methylhydroperoxide | 1 | 1 | 4 | 2 | | | 48.02 |
| MGLY | Methylglyoxal | 3 | 3 | 4 | 2 | | | 72.04 |
| N2O5 | Dinitrogen pentoxide | | | | 5 | 2 | | 107.95 |
| NO | Nitric oxide | | | | 1 | 1 | | 29.99 |
| NO2 | Nitrogen dioxide | | | | 2 | 1 | | 45.98 |
| NO3 | Nitrate radical | | | | 3 | 1 | | 61.97 |
| NTR1 | Simple organic nitrates | | 4 | 9 | 3 | 1 | | 119.07 |
| NTR2 | Multi-functional organic nitrates | | 4 | 9 | 4 | 1 | | 135.06 |
| O3 | Ozone | | | | 3 | | | 47.97 |
| OLE | Terminal olefin carbon bond (R-C=C) | 3 | 3 | 6 | | | | 42.07 |
| OPAN | Peroxyacyl nitrate (PAN compound) from OPO3 | 4 | 4 | 3 | 6 | 1 | | 161.00 |
| OPEN | Aromatic ring opening product (unsaturated dicarbonyl) | 4 | 4 | 4 | 2 | | | 84.05 |
| PACD | Peroxyacetic and higher peroxycarboxylic acids | 2 | 2 | 4 | 3 | | | 76.02 |
| PAN | Peroxyacetyl Nitrate | 2 | 2 | 3 | 5 | 1 | | 120.99 |
| PANX | C3 and higher peroxyacyl nitrate | 3 | 3 | 5 | 5 | 1 | | 135.02 |
| PAR | Paraffin carbon bond (C-C) | 1 | 5 | 12 | | | | 72.13 |
| PNA | Peroxynitric acid | | | 1 | 4 | 1 | | 78.97 |
| PRPA | Propane | 3 | 3 | 8 | | | | 44.09 |
| ROOH | Higher organic peroxide | | 4 | 10 | 2 | | | 90.09 |
| SO2 | Sulfur dioxide | | | | 2 | | | 64.04 |
| SULF | Sulfuric acid (gaseous) | | | 2 | 4 | | | 98.03 |
| TERP | Monoterpenes | 10 | 10 | 16 | | | | 136.21 |
| TOL | Toluene and other monoalkyl aromatics | 7 | 7 | 8 | | | | 92.13 |
| XOPN | Aromatic ring opening product (unsaturated dicarbonyl) | 5 | 5 | 6 | 2 | | | 98.07 |
| XYL | Xylene and other polyalkyl aromatics | 8 | 8 | 10 | | | | 106.15 |
| ECH4 | Emitted methane (to enable tracking seperate from CH4) | 1 | 1 | 4 | | | | 16.04 |
| I2 | Molecular iodine | | | | | | 2 | 253.80 |
| I2O2 | Diiodine dioxide | | | | 2 | | 2 | 285.78 |
| IXOY | Condensable iodine oxides | | | | 3 | | 2 | 301.77 |
| HOI | Hypoiodous acid | | | 1 | 1 | | 1 | 143.90 |
| HIO3 | Iodic acid | | | 1 | 3 | | 1 | 175.88 |
| INO3 | Iodine nitrate | | | | 3 | 1 | 1 | 188.87 |

**Table A-3. CB6r4 primary (unshaded) and secondary (shaded) photolysis rates (1/s) by solar zenith angle at 600 m MSL/AGL.**

| Reaction ID | Solar zenith angle (degree) | | | | | | | | | |
|---|---|---|---|---|---|---|---|---|---|---|
| | 0 | 10 | 20 | 30 | 40 | 50 | 60 | 70 | 78 | 86 |
| 1 | 1.01E-02 | 9.99E-03 | 9.77E-03 | 9.38E-03 | 8.75E-03 | 7.77E-03 | 6.30E-03 | 4.15E-03 | 2.09E-03 | 5.12E-04 |
| 8 | 4.26E-04 | 4.24E-04 | 4.19E-04 | 4.10E-04 | 3.94E-04 | 3.71E-04 | 3.33E-04 | 2.69E-04 | 1.79E-04 | 4.27E-05 |
| 9 | 4.55E-05 | 4.41E-05 | 3.99E-05 | 3.35E-05 | 2.54E-05 | 1.67E-05 | 8.78E-06 | 3.17E-06 | 9.20E-07 | 1.52E-07 |
| 21 | 8.79E-06 | 8.66E-06 | 8.26E-06 | 7.60E-06 | 6.64E-06 | 5.35E-06 | 3.78E-06 | 2.05E-06 | 8.81E-07 | 2.03E-07 |
| 27 | 1.88E-01 | 1.88E-01 | 1.86E-01 | 1.84E-01 | 1.79E-01 | 1.71E-01 | 1.56E-01 | 1.26E-01 | 8.22E-02 | 1.79E-02 |
| 28 | 2.32E-02 | 2.32E-02 | 2.31E-02 | 2.28E-02 | 2.23E-02 | 2.14E-02 | 1.98E-02 | 1.64E-02 | 1.12E-02 | 2.63E-03 |
| 38 | 5.54E-05 | 5.46E-05 | 5.23E-05 | 4.84E-05 | 4.26E-05 | 3.48E-05 | 2.52E-05 | 1.42E-05 | 6.30E-06 | 1.48E-06 |
| 43 | 1.74E-03 | 1.73E-03 | 1.68E-03 | 1.61E-03 | 1.49E-03 | 1.31E-03 | 1.04E-03 | 6.69E-04 | 3.29E-04 | 8.35E-05 |
| 47 | 8.47E-07 | 8.28E-07 | 7.70E-07 | 6.80E-07 | 5.57E-07 | 4.09E-07 | 2.54E-07 | 1.16E-07 | 4.20E-08 | 7.98E-09 |
| 50 | 7.02E-06 | 6.88E-06 | 6.46E-06 | 5.78E-06 | 4.84E-06 | 3.66E-06 | 2.36E-06 | 1.12E-06 | 4.16E-07 | 7.73E-08 |
| 56 | 9.53E-07 | 9.36E-07 | 8.81E-07 | 7.94E-07 | 6.72E-07 | 5.19E-07 | 3.47E-07 | 1.75E-07 | 7.05E-08 | 1.52E-08 |
| 88 | 6.02E-06 | 5.94E-06 | 5.68E-06 | 5.25E-06 | 4.61E-06 | 3.75E-06 | 2.68E-06 | 1.49E-06 | 6.52E-07 | 1.53E-07 |
| 92 | 3.29E-06 | 3.22E-06 | 3.01E-06 | 2.68E-06 | 2.22E-06 | 1.66E-06 | 1.06E-06 | 4.98E-07 | 1.85E-07 | 3.60E-08 |
| 97 | 4.35E-05 | 4.28E-05 | 4.08E-05 | 3.74E-05 | 3.24E-05 | 2.58E-05 | 1.78E-05 | 9.29E-06 | 3.78E-06 | 7.90E-07 |
| 98 | 4.85E-05 | 4.80E-05 | 4.62E-05 | 4.32E-05 | 3.87E-05 | 3.23E-05 | 2.38E-05 | 1.37E-05 | 6.19E-06 | 1.51E-06 |
| 106 | 6.51E-06 | 6.36E-06 | 5.89E-06 | 5.16E-06 | 4.16E-06 | 2.98E-06 | 1.76E-06 | 7.29E-07 | 2.30E-07 | 3.57E-08 |
| 109 | 2.20E-05 | 2.15E-05 | 2.01E-05 | 1.79E-05 | 1.48E-05 | 1.11E-05 | 6.96E-06 | 3.20E-06 | 1.15E-06 | 2.10E-07 |
| 111 | 6.13E-06 | 5.98E-06 | 5.51E-06 | 4.78E-06 | 3.81E-06 | 2.69E-06 | 1.56E-06 | 6.43E-07 | 2.06E-07 | 3.39E-08 |
| 114 | 9.13E-05 | 9.06E-05 | 8.84E-05 | 8.45E-05 | 7.82E-05 | 6.87E-05 | 5.50E-05 | 3.58E-05 | 1.78E-05 | 4.29E-06 |
| 116 | 2.36E-04 | 2.35E-04 | 2.29E-04 | 2.19E-04 | 2.04E-04 | 1.80E-04 | 1.46E-04 | 9.67E-05 | 4.92E-05 | 1.16E-05 |
| 125 | 1.16E-06 | 1.12E-06 | 1.02E-06 | 8.55E-07 | 6.50E-07 | 4.28E-07 | 2.27E-07 | 8.20E-08 | 2.34E-08 | 3.59E-09 |
| 126 | 1.02E-06 | 9.94E-07 | 9.02E-07 | 7.62E-07 | 5.83E-07 | 3.88E-07 | 2.08E-07 | 7.70E-08 | 2.25E-08 | 3.51E-09 |
| 154 | 2.96E-05 | 2.93E-05 | 2.84E-05 | 2.69E-05 | 2.45E-05 | 2.09E-05 | 1.60E-05 | 9.75E-06 | 4.60E-06 | 1.16E-06 |
| 64 | 9.53E-07 | 9.36E-07 | 8.81E-07 | 7.94E-07 | 6.72E-07 | 5.19E-07 | 3.47E-07 | 1.75E-07 | 7.05E-08 | 1.52E-08 |
| 90 | 6.02E-06 | 5.94E-06 | 5.68E-06 | 5.25E-06 | 4.61E-06 | 3.75E-06 | 2.68E-06 | 1.49E-06 | 6.52E-07 | 1.53E-07 |
| 156 | 7.04E-04 | 6.99E-04 | 6.84E-04 | 6.57E-04 | 6.12E-04 | 5.44E-04 | 4.41E-04 | 2.91E-04 | 1.46E-04 | 3.58E-05 |
| 188 | 1.51E-04 | 1.50E-04 | 1.47E-04 | 1.41E-04 | 1.31E-04 | 1.17E-04 | 9.45E-05 | 6.23E-05 | 3.13E-05 | 7.68E-06 |
| 189 | 8.04E-04 | 7.99E-04 | 7.82E-04 | 7.51E-04 | 7.00E-04 | 6.21E-04 | 5.04E-04 | 3.32E-04 | 1.67E-04 | 4.09E-05 |
| 193 | 8.04E-04 | 7.99E-04 | 7.82E-04 | 7.51E-04 | 7.00E-04 | 6.21E-04 | 5.04E-04 | 3.32E-04 | 1.67E-04 | 4.09E-05 |
| 209 | 1.73E-01 | 1.73E-01 | 1.72E-01 | 1.69E-01 | 1.65E-01 | 1.57E-01 | 1.44E-01 | 1.16E-01 | 7.58E-02 | 1.65E-02 |
| 210 | 1.02E-01 | 1.01E-01 | 9.87E-02 | 9.48E-02 | 8.84E-02 | 7.84E-02 | 6.36E-02 | 4.19E-02 | 2.11E-02 | 5.17E-03 |
| 212 | 1.88E-01 | 1.87E-01 | 1.83E-01 | 1.75E-01 | 1.64E-01 | 1.45E-01 | 1.18E-01 | 7.77E-02 | 3.91E-02 | 9.57E-03 |
| 217 | 1.71E-01 | 1.70E-01 | 1.69E-01 | 1.67E-01 | 1.62E-01 | 1.55E-01 | 1.41E-01 | 1.15E-01 | 7.46E-02 | 1.63E-02 |
| 223 | 2.54E-02 | 2.51E-02 | 2.42E-02 | 2.26E-02 | 2.02E-02 | 1.69E-02 | 1.25E-02 | 7.17E-03 | 3.23E-03 | 7.88E-04 |